AGU PUBLICATIONS

JGR

Journal of Geophysical Research: Atmospheres

RESEARCH ARTICLE
10.1002/2014JD022059

**Key Points:**
- Patterns of future rainfall changes were estimated for Hawaii
- A dry-wet anomaly pattern was downscaled with CMIP5 scenarios for Hawaii
- The likely scenario is a decrease (increase) in rainfall in dry (wet) regions

**Supporting Information:**
- Readme
- Figure S1
- Figure S2
- Figure S3

**Correspondence to:**
O. Elison Timm,
oelisontimm@albany.edu

**Citation:**
Elison Timm, O., T. W. Giambelluca, and H. F. Diaz (2015), Statistical downscaling of rainfall changes in Hawai'i based on the CMIP5 global model projections, *J. Geophys. Res. Atmos.*, *120*, 92–112, doi:10.1002/2014JD022059.

Received 22 MAY 2014
Accepted 27 NOV 2014
Accepted article online 3 DEC 2014
Published online 12 JAN 2015

# Statistical downscaling of rainfall changes in Hawai'i based on the CMIP5 global model projections

**Oliver Elison Timm[1], Thomas W. Giambelluca[2], and Henry F. Diaz[3]**

[1]Department of Atmospheric and Environmental Sciences, State University of New York at Albany, Albany, New York, USA, [2]Department of Geography, University of Hawai'i at Mānoa, Honolulu, Hawaii, USA, [3]NOAA/ESRL Cooperative Institute for Research in Environmental Sciences, University of Colorado Boulder, Boulder, Colorado, USA

**Abstract** Seasonal mean rainfall projections for Hawai'i are given based on statistical downscaling of the latest Coupled Model Intercomparison Project phase 5 (CMIP5) global model results for two future representative concentration pathways (RCP4.5 and RCP8.5). The spatial information content of our statistical downscaling method is improved over previous efforts through the inclusion of spatially extensive, high-quality monthly rainfall data set and the use of improved large-scale climate predictor information. Predictor variables include moisture transport in the middle atmosphere (700 hPa), vertical temperature gradients, and geopotential height fields of the 1000 and 500 hPa layers. The results allow for the first time to derive a spatially interpolated map with future rainfall change estimates for the main Hawaiian Islands. The statistical downscaling was applied to project wet (November–April) and dry (May–October) season rainfall anomalies for the middle and late 21st century. Overall, the statistical downscaling gives more reliable results for the wet season than for the dry season. The wet-season results indicate a pronounced dipole structure between windward facing mountain slopes and the leeward side of most of the islands. The climatically wet regions on the windward slopes of the mountain regions are expected to become wetter or remain stable in their seasonal precipitation amounts. On the climatically dry leeward sides of Kaua'i, O'ahu, Maui, and Hawai'i Island, future precipitation exhibits the strongest drying trends. The projected future rainfall anomaly pattern is associated with a circulation anomaly that resembles a shift in the position or strength of the subtropical high and the average location of extratropical troughs. These new results suggest that a negative trend dominates the area-averaged changes in the statistical downscaling over the Hawaiian Islands. However, the islands are expected to experience a greater contrast between the wet and dry regions in the future.

## 1. Introduction

In the last few decades, wet-season (November through April) rainfall for the Hawaiian Islands has exhibited a drying trend in excess of 10% of the mean [*Diaz and Giambelluca*, 2012]. Climate projections for business as usual and moderate emissions mitigation scenarios derived from the Coupled Model Intercomparison Project phase 3 (CMIP3) and phase 5 (CMIP5) suggest a general wet-season drying trend to the end of the 21st century for Hawai'i, according to the two most recent Intergovernmental Panel on Climate Change (IPCC) assessment reports [*Intergovernmental Panel on Climate Change (IPCC)*, 2007, 2013, Annex I Fig. AI74]. Higher precipitation is projected over the central and eastern tropical Pacific, but the subtropical regions around the Hawaiian Islands show a negative precipitation change of small amplitude [*Power et al.*, 2012]. These projected regional rainfall changes represent mostly open-ocean conditions and as such cannot be used as reliable estimates for changes in the water budget calculations over land.

*Nullet and McGranaghan* [1988] used the station network of rain gauge stations in Hawai'i to show that a rainfall enhancement factor of 3.4 is likely to describe the net effects orographic effects on the rainfall budget. This statewide perspective is integrated over spatial rainfall gradients that range between 250 mm and more than 11,000 mm annual total rainfalls within horizontal length scales of 10–100 km and vertical scales of the order of 1–4 km. With the advances in satellite remote sensing of precipitation over oceans it has become possible to measure the general effects of small islands on the enhancement (or reduction) of precipitation compared with the open-ocean surroundings [*Sobel et al.*, 2011]. It was found that the dimensions of islands and their geometry and orographic features lead to different enhancement effects. It is therefore not

permissible to apply simple bias correction and scaling principles to downscale coarse-resolution precipitation products of the CMIP models, which exclude orographic and thermal effects of the islands. The interaction between trade winds and islands drastically changes the cloud and rain formation processes [*Leopold*, 1949; *Rasmussen et al*., 1989; *Xie et al*., 2001; *Yang and Chen*, 2003; *Lauer et al*., 2013]. Past project campaigns have studied island weather and airflow interactions by means of field observations and theoretical numerical models. These projects target the meteorological aspects of specific rain and cloud formation processes and are insightful for understanding rain formation processes on synoptic time scales [e.g., *Lavoie*, 1967; *Takahashi*, 1977; *Rasmussen et al*., 1989; *Smolarkiewicz et al*., 1988; *Chen and Nash*, 1994; *Kodama and Barnes*, 1997; *Zhang et al*., 2005; *Yang and Chen*, 2008; *Hartley and Chen*, 2010].

Despite the complexity of the processes involved, linearized approaches to the full three-dimensional numerical simulations of orographic precipitation [*Smolarkiewicz et al*., 1988; *Smith and Barstad*, 2004; *Kirshbaum and Smith*, 2009] have been applied to the problem of understanding general features of tropical island precipitation. According to these theoretical concepts, the horizontal and vertical length scales together with the flow characteristics such as mean wind speed and stratification play a dominant role for the formation and spatial distribution of orographically forced rainfall. Future rainfall changes in Hawai'i can therefore be considered from two perspectives: one that would attempt to understand the changes in flow dynamics (mechanically and thermodynamically forced precipitation) or one that would pursue a statistical climate diagnostics that combines the large-scale circulation pattern with rainfall statistics in Hawai'i [e.g., *Timm and Diaz*, 2009]. The latter approach is applied in this study.

Refinements of the global climate model outputs toward spatial resolutions relevant to resource managers and policymakers have been done with statistical and dynamical downscaling methods. For example, the recent efforts from the North American Regional Climate Change Assessment Program [*Mearns et al*., 2009] and the NASA Earth Exchange [*Thrasher et al*., 2013] have produced downscaled climate projections for the continental U.S. Remote locations like the Hawaiian Islands have not been included in such concerted efforts to obtain a detailed view on the regional pattern of climate change, and much of the current information is more or less a direct output from the coarse-resolution CMIP5 models. For example, *Wuebbles et al*. [2014] present projected changes in the mean rainfall for the state of Hawaii. Given the very different rainfall climatologies between leeward and windward sides of the islands [*Giambelluca et al*., 2013] (see also Figure S1 in the supporting information) and their different physical rain formation processes, it is clear that refined estimates are needed for local environmental impact studies in Hawai'i [*Hobbelen et al*., 2012; *Judge et al*., 2012; *LaPointe et al*., 2012; *Tanaka et al*., 2013].

In previous studies, we explored how the major circulation patterns that affect Hawaiian Islands rainfall might change and provided estimates of the concomitant changes in seasonal mean rainfall [*Timm and Diaz*, 2009, hereinafter TD09] and the frequency of heavy rain events [*Elison Timm et al*., 2011, 2013]. Here we have updated seasonal mean rainfall projections using the latest CMIP5 model scenarios based on two future representative concentration pathways (RCP4.5 and RCP8.5). In this study we have improved the spatial information content of our statistical downscaling (SD) method through the introduction of the Rainfall Atlas of Hawai'i station data sets [*Giambelluca et al*., 2013] and the use of improved large-scale climate predictor information. Whereas TD09 restricted large-scale circulation information to the meridional surface winds, in this study we work with a multivariate circulation data set that includes moisture transport in the middle atmosphere (700 hPa), vertical temperature gradients, and geopotential height fields of the 1000 and 500 hPa layers.

In this paper we briefly review the SD method and the input data in section 2. The results are presented in section 3. In section 4 we discuss the spatial and seasonal features of the projected rainfall changes and their uncertainties. We end our paper with a summary of the most robust climate change signals and some cautionary notes on the further use of projected rainfall changes and their uncertainties in decision-making processes and environmental impact studies.

## 2. Methods and Data

### 2.1. Data

In this study gap-filled monthly rainfall data from the Rainfall Atlas of Hawai'i [*Giambelluca et al*., 2013] were aggregated into wet (November–April) and dry (May–October) season rainfall totals and the annual mean

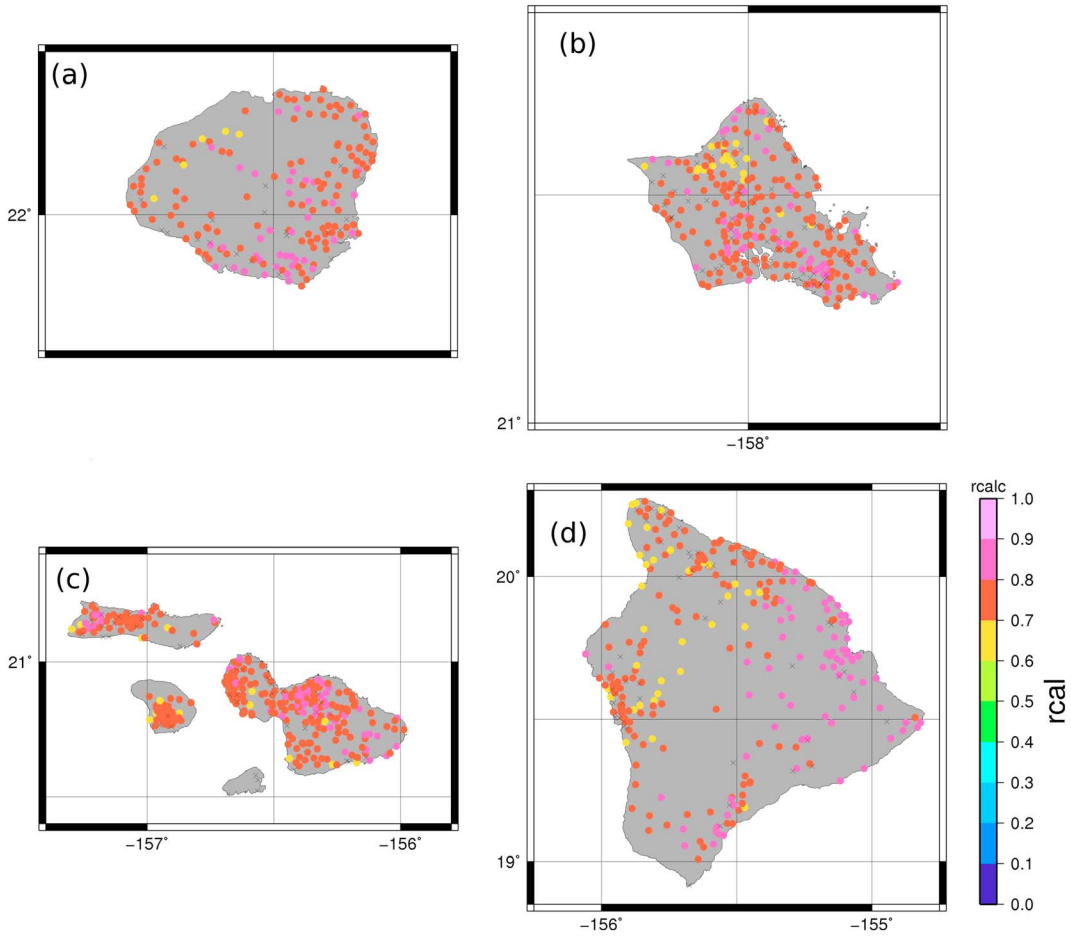


**Figure 1.** Statistical downscaling (SD) calibration results obtained with Monte Carlo resampling using 200 realizations (15 random years from the period 1978–2007) for the wet season. Colored dots show the mean calibration correlation coefficient (Rcal) between the observed rainfall anomalies and the SD estimates at each station: (a) Kaua'i; (b) O'ahu; (c) Moloka'i, Lāna'i, and Maui; (d) Hawai'i Island. Note that stations with incomplete data coverage in 1978–2007 were excluded for this Monte Carlo test.

time series. In total we used 948 (915 dry season) of the available 1104 stations for the statistical downscaling calculations (see Figures 1–3). In the original data set, monthly mean rainfall amounts are available for the years 1920–2007. As explained below, for the statistical downscaling model parameter estimation, we used the years 1978–2007.

For the large-scale climate diagnostics, monthly mean National Centers for Environmental Prediction (NCEP)/National Center for Atmospheric Research (NCAR) reanalysis data were used. The monthly mean data were first aggregated into the Hawaiian wet and dry seasons (November–April and May–October, respectively). In this study, we used data from the years 1978–2007. Earlier results [*Elison Timm et al*., 2013] have shown that changes in the data assimilation—most likely due to incorporation of the satellite remote sensing data into the data input stream—increase the quality of reanalysis for Hawai'i and the surrounding region beginning around the late 1970s compared with the earlier period. For the downscaling model parameter estimation (hereafter referred to as "calibration") it is advantageous to work with the large-scale circulation data with relatively low uncertainties. The end year, 2007, was determined by the rainfall data limitations at the time of the study. The monthly mean gridded (2.5° × 2.5°) reanalysis data sets for the area 180°E–240°E (Dateline 120°W) and 10°S–40°N were extracted from the global fields and seasonally averaged.

Our choice of domain size and climatic variables used as large-scale predictors in the statistical downscaling process is based on a number of criteria. First and foremost, the climate variables should have a strong

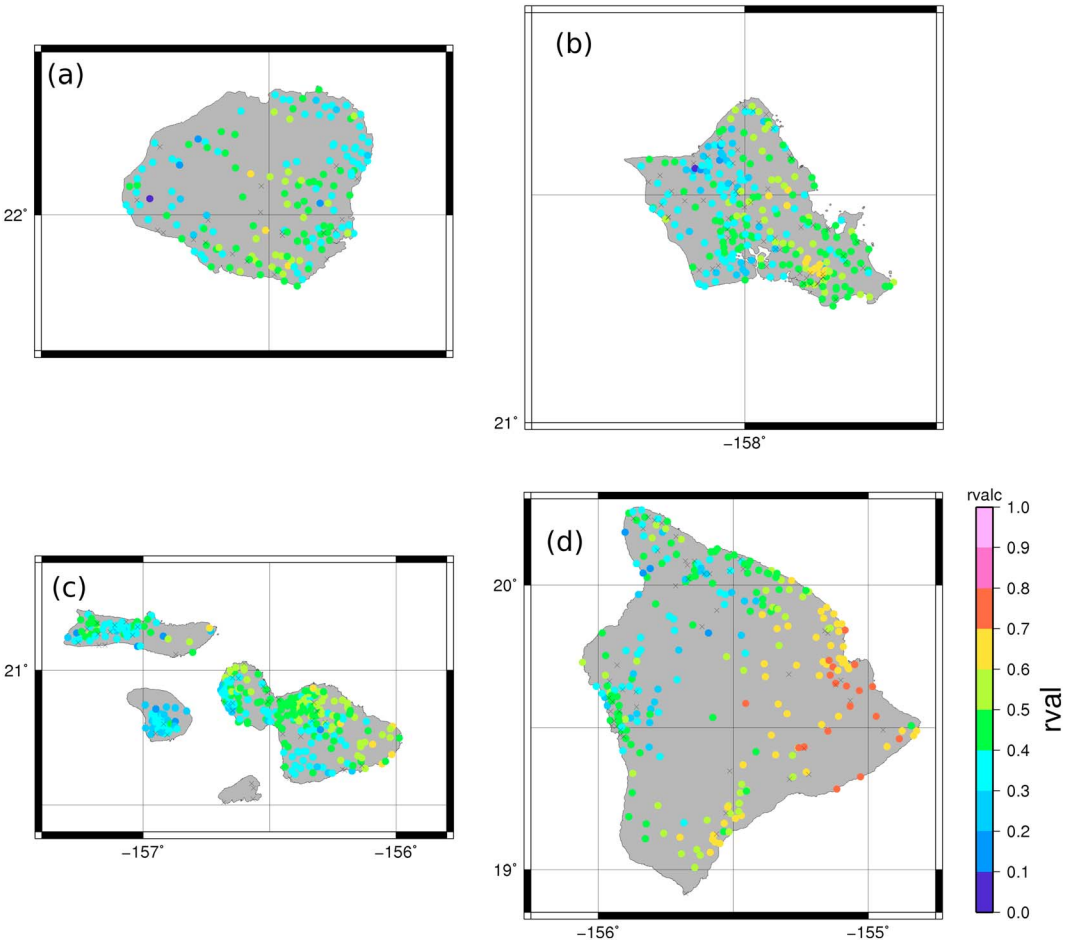


**Figure 2.** Statistical downscaling (SD) cross-validation results for the wet season. For each Monte Carlo subsample we used observed rainfall anomalies of years excluded from the model parameter fitting. The means of the correlation coefficients between observed and SD estimated rainfall anomalies are shown as colored dots for each station.

physical connection to the local rainfall processes. The stability of the atmosphere, moisture content, and wind directions are found to be the most important factors for rain formation processes on the larger scale.

Table 1 summarizes the circulation variables used in the downscaling process as large-scale predictor information for station rainfall. Moisture fluxes were calculated from the wind components and specific humidity on the 700 hPa level. Geopotential heights at 500 hPa were converted to anomalies with respect to the areal average in the selected regional domain. This was done to treat the NCEP data and CMIP5 data in the same manner. In this way we avoid artifacts resulting from the global increase in the 500 hPa level in the future warming scenarios, which could bias the downscaling results. Note, however, that the vertical temperature gradient between the 1000 and 500 hPa levels was not corrected for the global increase in the vertical stability (as seen in future climate change scenarios). The domain size has been chosen in our previous studies based on a compromise between a local (and thus more direct control of rainfall) domain over the islands and a larger domain that is suitable for the projection of coarser-scale CMIP5 model simulation scenarios.

Future projections of climate change from the CMIP5 database were retrieved from the official Earth System Grid archives [*Taylor et al*., 2012]. Two representative concentrations pathways (RCP) are used in this study: RCP4.5 and RCP8.5, where the number indicates the radiative forcing equivalent (in $W/m^2$) induced by the anthropogenic forcing by the end of the 21st century. The years 1975–2005 from historical scenario runs from the CMIP5 models were used to define mean circulation conditions in the models, from which circulation anomalies were derived for the future model runs. At the time of the research, we were able to work with an ensemble of 32 models (see Table 2), using a single simulation from each model.

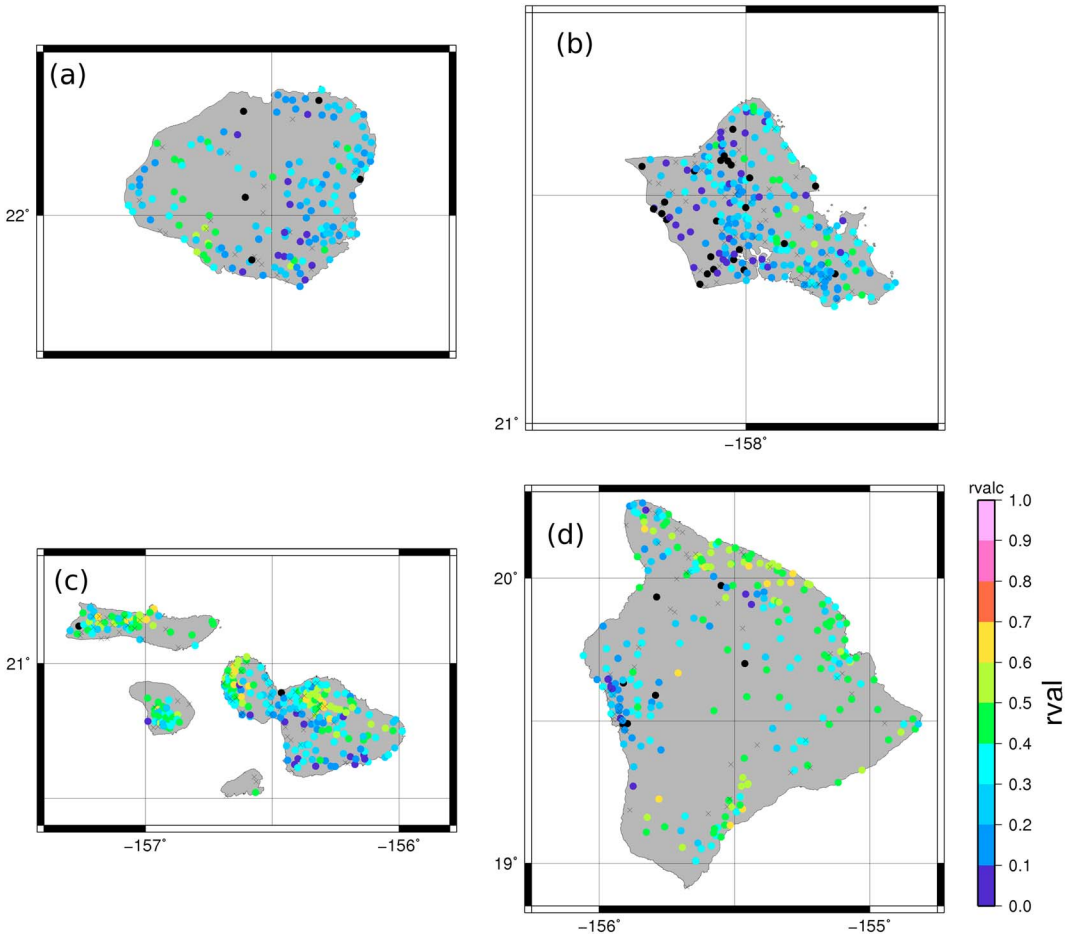


**Figure 3.** Same as in Figure 2 but showing results for the validation of the dry season.

### 2.2. Statistical Downscaling Method

The downscaling method follows the same procedure as described in TD09. Similar statistical downscaling techniques have been described in the literature [e.g., *Wilby et al*., 2004; *Benestad*, 2001; *Wang and Zhang*, 2008; *Maraun et al*., 2010; *Sobie and Weaver*, 2012].

#### 2.2.1. Composite Circulation Pattern

The first steps in developing our statistical downscaling model starts with a classification method that distinguishes below and above average rainfall seasons at each station. First, for each station the seasonal rainfall amounts were converted into percentages with respect to the station's 1978–2007 climatological mean value and sorted in ascending order. For each station, we take the years of the eight lowest and eight highest rainfall seasons to form composite maps of the seasonal mean NCEP/NCAR reanalysis data sets. The composite maps depict the average large-scale circulations associated with below and above average rainfall conditions at the individual stations. For the downscaling it was decided to work with the

**Table 1.** Large-Scale Circulation Variables Used for the Composite Analysis

| No | Label | Variable Description |
|---|---|---|
| 1 | zg500 | Geopotential height at 500 hPa |
| 2 | zg1000 | Geopotential height at 1000 hPa |
| 3 | dt | Air temperature difference 1000 hPa minus 500 hPa |
| 4 | su700 | Zonal moisture transport in 700 hPa |
| 5 | sv700 | Meridional moisture transport in 700 hPa |

**Table 2.** CMIP5 Models Used in the Multimodel Ensemble Downscaling

| Modeling Center or Group | Institute ID | Model Name |
|---|---|---|
| Commonwealth Scientific and Industrial Research Organization (CSIRO) and Bureau of Meteorology (BOM), Australia | CSIRO-BOM | ACCESS1.0<br>ACCESS1.3 |
| Beijing Climate Center, China Meteorological Administration | BCC | BCC-CSM1.1<br>BCC-CSM1.1(m) |
| College of Global Change and Earth System Science, Beijing Normal University | GCESS | BNU-ESM |
| Canadian Centre for Climate Modelling and Analysis | CCCMA | CanESM2 |
| National Center for Atmospheric Research | NCAR | CCSM4 |
| Community Earth System Model Contributors | NSF-DOE-NCAR | CESM1(BGC)<br>CESM1(CAM5) |
| Centro Euro-Mediterraneo per I Cambiamenti Climatici | CMCC | CMCC-CESM<br>CMCC-CMS |
| Centre National de Recherches Météorologiques/Centre Européen de Recherche et Formation Avancée en Calcul Scientifique | CNRM-CERFACS | CNRM-CM5 |
| LASG, Institute of Atmospheric Physics, Chinese Academy of Sciences and CESS,Tsinghua University | LASG-CESS | FGOALS-g2 |
| LASG, Institute of Atmospheric Physics, Chinese Academy of Sciences | LASG-IAP | FGOALS-s2 |
| The First Institute of Oceanography, SOA, China | FIO | FIO-ESM |
| NOAA Geophysical Fluid Dynamics Laboratory | NOAA GFDL | GFDL-CM3/-ESM2G/-ESM2M |
| National Institute of Meteorological Research/Korea Meteorological Administration | NIMR/KMA | HadGEM2-AO |
| Met Office Hadley Centre (additional HadGEM2-ES realizations contributed by Instituto Nacional de Pesquisas Espaciais) | MOHC (and INPE) | HadGEM2-CC<br>HadGEM2-ES |
| Institute for Numerical Mathematics | INM | INM-CM4 |
| Institut Pierre-Simon Laplace | IPSL | IPSL-CM5A-LR<br>IPSL-CM5A-MR |
| Japan Agency for Marine-Earth Science and Technology, Atmosphere and Ocean Research Institute (The University of Tokyo), and National Institute for Environmental Studies | MIROC | MIROC-ESM/-ESM-CHEM |
| Atmosphere and Ocean Research Institute (The University of Tokyo), National Institute for Environmental Studies, and Japan Agency for Marine-Earth Science and Technology | MIROC | MIROC5 |
| Max-Planck-Institut für Meteorologie (Max Planck Institute for Meteorology) | MPI-M | MPI-ESM-MR<br>MPI-ESM-LR |
| Meteorological Research Institute | MRI | MIR-CGCM3 |
| Norwegian Climate Centre | NCC | NorESM1-M<br>NorESM1-ME |

circulation anomalies with respect to a 1978–2007 climatology. The high (low) anomaly patterns serve as above (below) average rainfall indicators in the large-scale circulation using the variables listed in Table 1. That is, each station is associated with a unique set of five-multivariate composite pattern for the above average rainfall and five for the below average rainfall years (ten for each station).

#### 2.2.2. Large-Scale Circulation Predictor Time Series

After each station was assigned its composite pattern, we use the mathematical vector-projection method to derive for each year an index that measures the correlation and amplitude of the observed circulation anomaly with the composite pattern. We decided to perform the vector projection with the individual climate field variables. Thus, for a given station and a given observation year, we obtain 10 scalar values that describe the state of the circulation with respect to the high and low composite patterns. The vector projection is applied to the seasonal anomalies of the NCEP/NCAR reanalysis fields (anomalies relative to the 1978–2007 mean). This results in 10 time series indices for the years 1978–2007.

It should be noted that the vector-projection indices contain redundant information due to the physical linkages between geopotential heights, winds, vertical temperature gradients, and moisture transports and because the high and low composite patterns exhibit strong negative spatial correlation. Furthermore, year-to year variations in wet-season rainfall over Hawai'i appear spatially organized, despite the complexity of the climatological rainfall pattern (see Figure S1 in the supporting information). This is reflected in the fact that the vector-projection indices share a large portion of variance among all rainfall stations.

**Table 3.** Cross Validation of the SD Method Using Low Precipitation for Calibration and High-Precipitation Years for Validation and Vice Versa[a]

| Calibration/Validation | Island | RMSE PERS (%) | RMSE SD (%) | SIGN SD (%) | Number of Stations |
|---|---|---|---|---|---|
| Low/high | HA | 67 (37) | 57 (24) | 86 (97) | 240 (212) |
| | MA | 72 (63) | 66 (51) | 73 (82) | 289 (256) |
| | OA | 71 (56) | 64 (48) | 84 (73) | 232 (230) |
| | KA | 65 (47) | 63 (45) | 49 (−1) | 152 (147) |
| High/low | HA | 67 (38) | 73 (29) | −1 (79) | 238 (232) |
| | MA | 72 (63) | 49 (46) | 86 (55) | 291 (263) |
| | OA | 72 (57) | 62 (51) | 70 (72) | 233 (233) |
| | KA | 66 (46) | 43 (40) | 98 (88) | 148 (145) |

[a]Statistics are based on the station samples in each island region (sample size is given in the column "number of stations"). Columns "RMSE PERS" and "RMSE SD" show the root-mean-square error for the persistence estimates versus observed and the downscaled estimates versus observed, respectively, for the subsampled years mean. Values are in percent rainfall anomalies. "SIGN SD" measures the agreement in downscaled and observed sign of anomalies. Note that 0% indicates that half of the station estimates agree in their sign. Positive (negative) values indicate positive (negative) correlation in the signs. Numbers in cells are for the wet season and in parenthesis for the dry season.

In situations where multivariate data sets contain redundant information, principal component analysis (PCA) offers a universal method to compress a large fraction of the total variability into a few leading eigenmodes. Here we deploy the PCA mostly for two reasons: (1) to reduce the number of time series that describe the rainfall-large-scale-circulation relationships and (2) to prewhiten the time series that will be used as predictors in the multiple linear regression step of the statistical downscaling (see below).

The PCA was applied to four island regions (Kaua'i, KA; O'ahu, OA; Maui, MA; Hawai'i Island, HA) separately. For example, we applied the PCA to the vector-projection indices from Hawai'i Island stations using the wet-season composite results. The PCA compresses the variability of the multivariate data set into a set of eigenmodes with the four leading modes representing more than 90% of the total variability for the wet season (Table 3). The principal component (PC) time series of first four modes are used as large-scale climate predictors in the next step of the statistical downscaling. Six PCA modes were used for the dry season; the larger number of modes needed to explain about 90% of the total variability indicates that dry-season rainfall variability patterns are more complex and less organized through large-scale processes than wet-season rainfall variations.

It should be noted that the PCA compression, in effect, determines the spatial degrees of freedom for the downscaled precipitation changes. The resulting principal component time series are subsequently used as predictors for rainfall anomalies at individual stations. For each station, we applied multiple linear regressions (MLR), using the PCA time series as independent variables (predictors), to obtain estimates of the rainfall anomalies from the large-scale predictor information. Thus, instead of having a set of individual predictor time series at each station, the predictor information is the same for all stations within one island group.

#### 2.2.3. Cross Validation of the Statistical Downscaling Model

Having found the composite pattern and the corresponding large-scale predictor time series, the MLR was first fitted using all sample years 1978–2007. An analysis of variance *F* test, which measures the ratio of explained to unexplained variance in the regression model, was used to measure the statistical significance. The majority of stations passed the *F* test. Furthermore, most stations had statistically significant correlations (Rcal) between estimated and observed rainfall anomalies for the same set of years used in fitting the MLR. However, in order to measure the correlation skill with more conservative methods, independent samples must be used. Since high-quality observations are limited, we applied a Monte Carlo (MC) technique [e.g., *Wilks*, 2006, Section 5.3.2], in which we randomly selected a set of 15 calibration years (without repetition) from the years 1978–2007. The remaining years were used for cross validation. This was repeated 200 times. This procedure is applicable for obtaining a conservative estimate of the correlation skill on interannual time scales.

Future rainfall change projections usually consider changes in the climatological mean over 20 or 30 years, and thus, one should ideally test the performance of the statistical model also on these longer time scales. The previous Monte Carlo test does not allow for systematic differences in the calibration and validation sample mean statistics, since random subsamples will have the same sample mean precipitation values.

We also conducted a cross validation similar to that done in TD09, where we used the earlier years (1958–1976) for validation to obtain a more conservative test of the SD model. The latter cross-validation results show a considerable decrease in the correlation between downscaled and observed rainfall compared with the Monte Carlo cross validation. An immediate interpretation would suggest that the statistical relationships that were estimated on (mainly) variances in the interannual to decadal time scales are different on multidecadal time scales. However, as we have shown in a related study [*Elison Timm et al*., 2013], moisture variables from reanalysis data sets are less reliable prior to the satellite era. The lost downscaling skill during the earlier years may be in part attributable to the loss in accuracy of the earlier reanalysis data [*Brands et al*., 2012] and/or to a real change in the strength of the leading modes of variability in the atmosphere [*Diaz et al*., 2001]. In particular, the long-term mean precipitation changes are affected by differences in the input data stream in the data assimilation process. In the end, the test remained inconclusive for measuring the skill of the statistical downscaling on 30 year mean changes.

As a final attempt to test whether the downscaling has "predictive skill" for mean precipitation changes, we split the 30 year data into the 15 highest and 15 lowest rainfall (averaged over the island stations) years and used them for cross validation. The root-mean-square error (RMSE) is calculated for each island group and for each season using the 15 year means of the estimated rainfall anomalies (in units of percent of subsample mean rainfall). The RMSE is calculated from the station sample relative to the observed means. For comparison, the RMSE of the persistence model (no change relative to the calibration mean) is given.

The sign-test measures the number of agreements in the sign of the estimated rainfall anomaly and the observed anomaly. The sign function was used to transform anomalies into −1 and +1 values for negative and positive anomalies, respectively. Then the sum of the product of the sign values (observed times downscaled) is divided by the total number of stations and expressed in percent. It should be noted that the percentage of stations where downscaled and observed changes agree in sign can range from −100 to 100%. Thus, the higher the number above zero, the better the agreement.

## 3. Results

### 3.1. Cross Validation of the Statistical Downscaling Model

Figure 1 shows the mean of the correlation coefficients for each station from SD models fitted with the 200 MC samples. Very high correlations between observed and estimated rainfall anomalies are found at all stations (almost all significant at the 5% level). On Maui and Hawai'i Island (Figures 1c and 1d) a spatial pattern emerges that indicates higher correlations in regions with high rainfall. Even for the dry leeward sides of islands, correlation values above 0.6 are found, explaining more than 30% of the variability in the observations. Similar results are also seen in the dry season (not shown).

More informative than the fitted calibration skill is the result from the correlation with the independent sample years. Figure 2 shows the mean correlation of the MC cross validation for the wet season. The correlation is, in most regions, lower, and a clear spatial pattern is observed. Higher correlations are obtained in the regions with high rainfall rates and frequent rain events. The lowest correlations are found in the dry regions of the islands, in particular the leeward sides; in fact the climatological mean precipitation amount and the explained variance of the cross correlation are correlated. Only a few stations show no correlation in the cross validation. The statistical downscaling skill of dry-season rainfall (Figure 3) is lower than that of the wet season. The small-scale nature of rain-producing synoptic disturbances and their infrequent appearance during the summer season make it more difficult to link rainfall to the large-scale seasonal mean circulation, as we have previously noted (TD09). Projections in many dry regions are not statistically robust, and cross-validated correlations are near zero (Figure 3).

The calibration with the data divided into equal-sized samples with the lowest and highest rainfall anomaly years (each 15 years) and the remaining data withheld for cross validation mimics a test of the downscaling model for reproducing different climate means. (We note that one must be careful in the statistical characterization of these subsamples. Here we assume that the subsamples are from the same climate state.) Table 3 summarizes the main results from this test. In all except one case, the RMSE of the downscaling model is smaller than the persistence model.

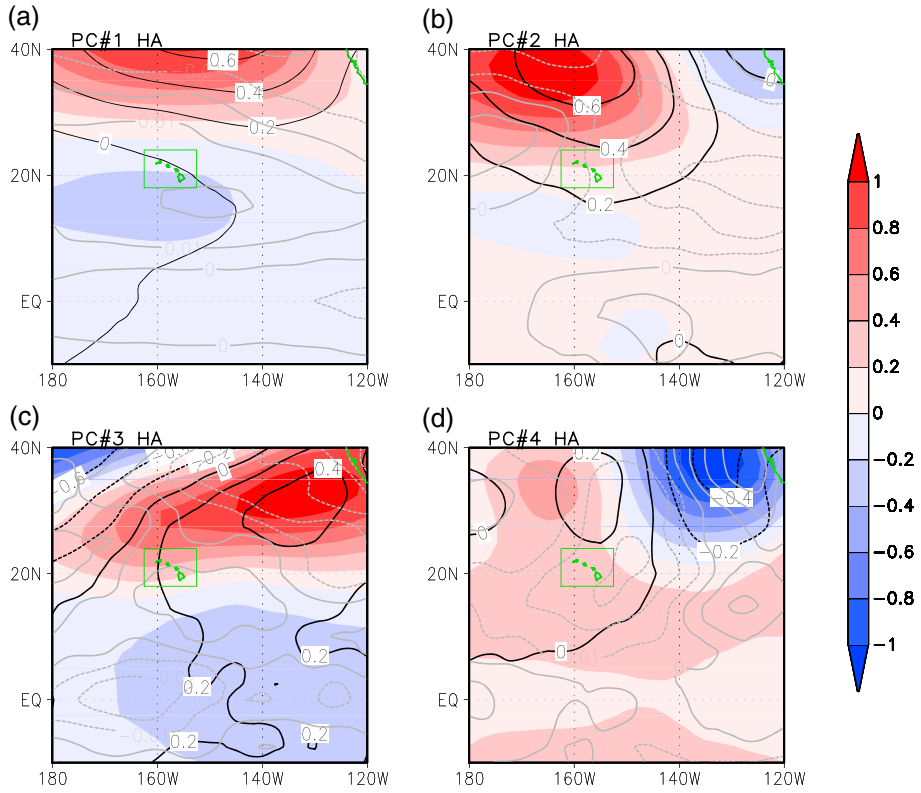


**Figure 4.** Analysis of the large-scale circulation pattern for Hawai'i Island during the wet season: Associated regression pattern in the 500 hPa geopotential height field (colors in m/stddev (PC)) and the 1000 hPa geopotential heights (contours, in 0.2 m/stddev (PC)) intervals). In gray are indicated contours for the regression pattern of the 1000–500 hPa temperature difference (K/stddev (PC)). Four leading PC time series were used: (a) PC 1; (b) PC 2; (c) PC 3; and (d) PC 4. Note that the PC time series have different standard deviations (40, 20, 12, and 10).

The sign test measures the number of agreements in the sign of the estimated rainfall anomaly and the observed anomaly. In general, high positive percentage numbers were found (Table 3), indicating that the majority of stations have the same sign in the observed and SD estimated anomalies. A few exceptions are noted: Kaua'i failed the high rainfall cross-validation sign test for the dry season; for Hawai'i Island, the sign test revealed low downscaling skills for the wet season when attempting to apply the SD model to the years with negative rainfall anomalies. It should be noted that the years were categorized based on station-averaged rainfall anomalies, and not all stations have experienced large rainfall anomalies. Overall, it is concluded that the method applied here to statistically downscale future rainfall changes is useful for projecting circulation-driven changes in the rainfall pattern in Hawai'i. The confidence in the projected changes is higher for the wet season than for the dry season. While the sign of the projected anomalies is likely to be correct, the absolute amplitude of the changes has to be considered with caution and should be compared with dynamical regional modeling results [*Lauer et al.*, 2013; *Zhang et al.*, 2012].

### 3.2. Large-Scale Circulation Anomalies

We illustrate the large-scale circulation anomalies here for the wet season using Hawai'i Island and Kaua'i as examples (similar patterns are found for O'ahu and Maui Nui). The regression pattern associated with the first PC time series for Hawai'i Island (Figure 4) and Kaua'i (Figure 5) have a north-south dipole in the 500 hPa geopotential height field, with a resemblance to the Pacific-North American (PNA) pattern: lower pressure in the northern (extratropical) sector is associated with higher pressure in the subtropical and tropical central parts of the domain. Similar features are observed near the surface in the 1000 hPa geopotential field. The PC time series of the first PCA mode has the strongest correlation with the PNA and El Niño–Southern Oscillation (ENSO) (NINO3.4) indices (over the years 1979–2007 used here; see Figure 6 and Table 4). The corresponding meridional and zonal components of the moisture transport in 700 hPa are shown in Figures 7 and 8 for

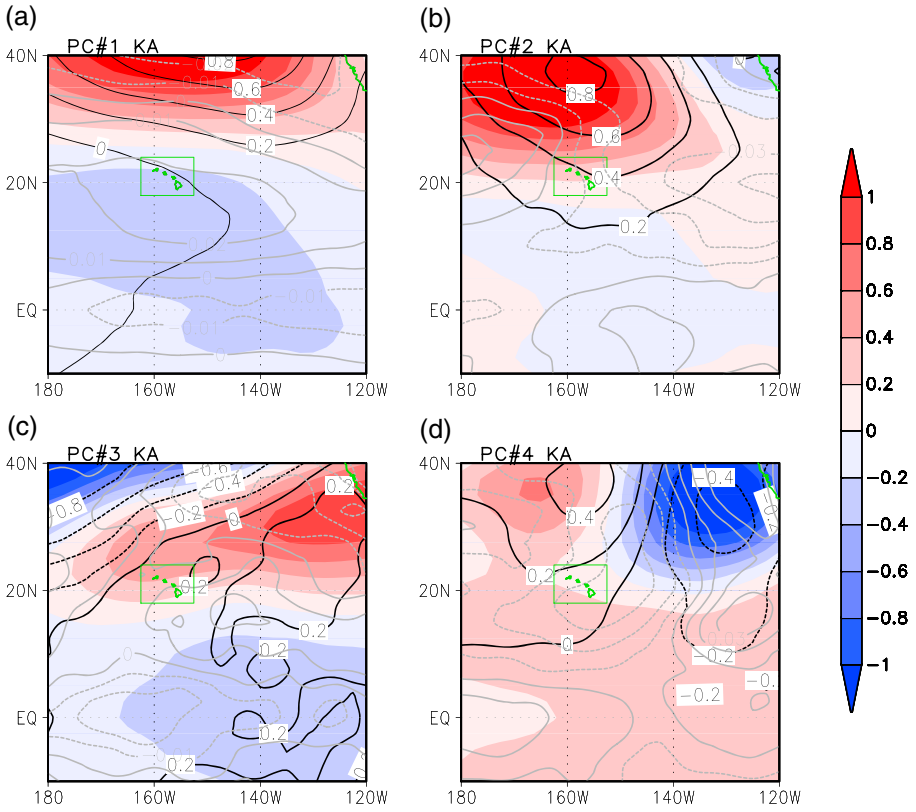


**Figure 5.** Same as Figure 4 but for the island of Kaua'i during the wet season.

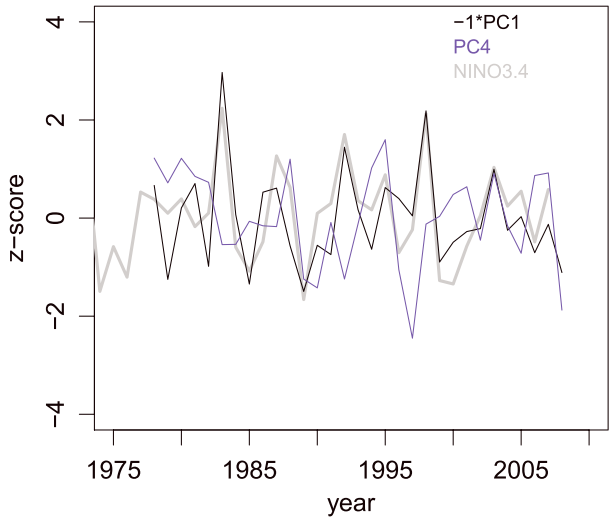


**Figure 6.** Principal component (PC) time series for Hawai'i Island and large-scale circulation indices for the wet-season months (November–April). The first and fourth PC time series are shown in black and blue, respectively. The NINO3.4 time series (gray) is shown for comparison. Note that PC 1 time series was inverted in sign to stress the correlation with ENSO. (The associated regression pattern in Figures 4a and 7a show anomalies representing La Niña years).

Hawai'i Island and Kaua'i, respectively. The transport anomalies in the extratropical regions closely follow the expected geostrophic wind anomalies in the pressure fields. This suggests that the dynamic component plays a crucial role in the total moisture transport variability. Comparing regression patterns associated with the four PCA modes, the regression patterns need not be orthogonal despite the orthogonality constraints of the PC time series. In fact, the regression pattern of PC 3 projects onto the ENSO-teleconnection pattern and the PNA pattern as well, and the time series of PC 3 is weakly correlated with PNA and NINO3.4 index. (Figure 6 and Table 4). These results confirm the commonly well-known fact that ENSO and PNA are the most important large-scale circulation modes for year-to-year rainfall variability in Hawai'i [*Chu*, 1995; *Chu and Chen*, 2005]. PC 4 and PC 2 are not correlated with ENSO

**Table 4.** Correlation Between Principal Component Time Series and NINO3.4 and PNA Index[a]

| | HA | | | | KA | | | |
|---|---|---|---|---|---|---|---|---|
| | PC 1 | PC 2 | PC 3 | PC 4 | PC 1 | PC 2 | PC 3 | PC 4 |
| NINO3.4 | −0.79 | 0.11 | −0.44 | 0.07 | −0.82 | 0.01 | −0.42 | −0.14 |
| PNA | −0.68 | 0.12 | 0.37 | 0.20 | −0.67 | 0.18 | 0.32 | −0.15 |

[a]Data from the wet-season years 1978–2007 are used. HA and KA denote the PC time series of the Hawai'i Island and Kaua'i.

and the PNA index, and the large-scale circulation anomalies do not project onto the ENSO/PNA teleconnection pattern. In particular, PC 4 is associated with a pronounced east-west dipole in the central and eastern extratropical/subtropical Pacific. Further, this mode is associated with large anomalies in the vertical temperature gradient centered over the Hawaiian Islands and moisture transport anomalies that follow the pressure-driven wind anomalies, which result in meridional transport anomalies northeast of the islands. In the next section, it will be shown that this circulation mode is an important component of the future climate change signal in the CMIP5 future scenarios. It should also be noted that moisture transport anomalies are larger in the tropics than in the extratropics due to the larger amplitude of changes in the moisture content.

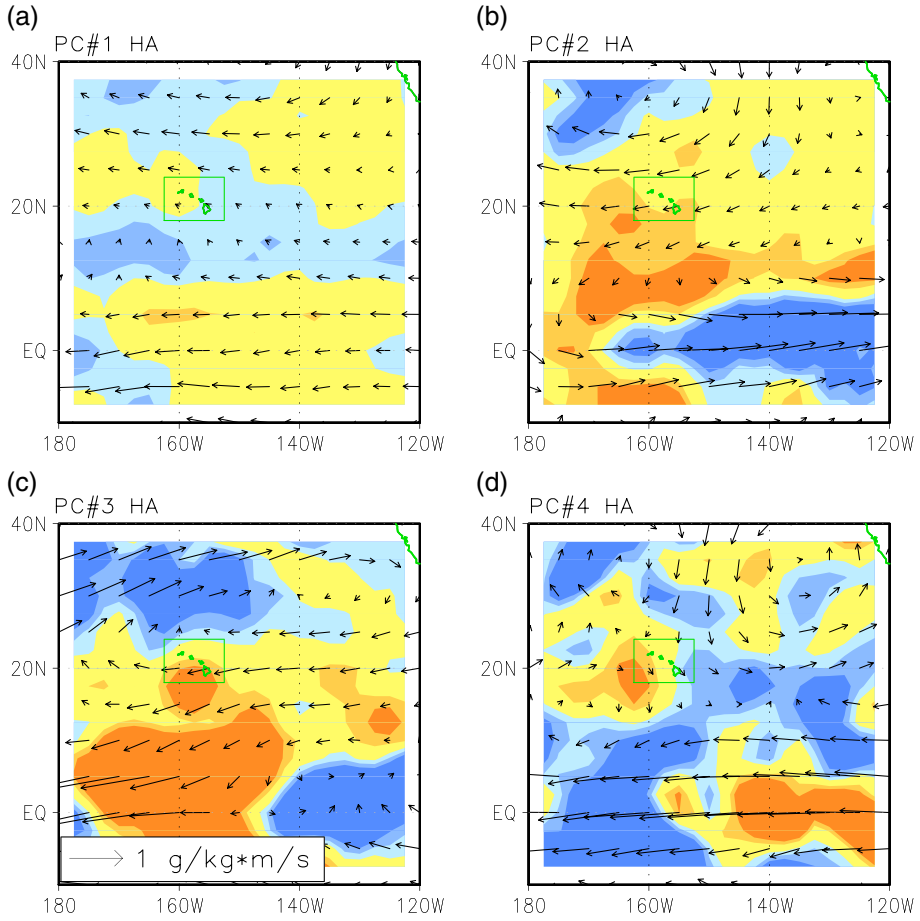


**Figure 7.** Regression pattern for the Hawai'i Island during the wet season showing the moisture transport anomalies at 700 hPa level associated with the four leading modes in the predictor time series. Four leading PC time series were used: (a) PC 1; (b) PC 2; (c) PC 3; and (d) PC 4. Note that the PC time series have different standard deviations (40, 20, 12, and 10, respectively). The length of the vector at the bottom indicates the magnitude of the change associated with one standard deviation in the PC time series. Blue and yellow/orange shadings illustrate the regions with convergence and divergence, respectively.

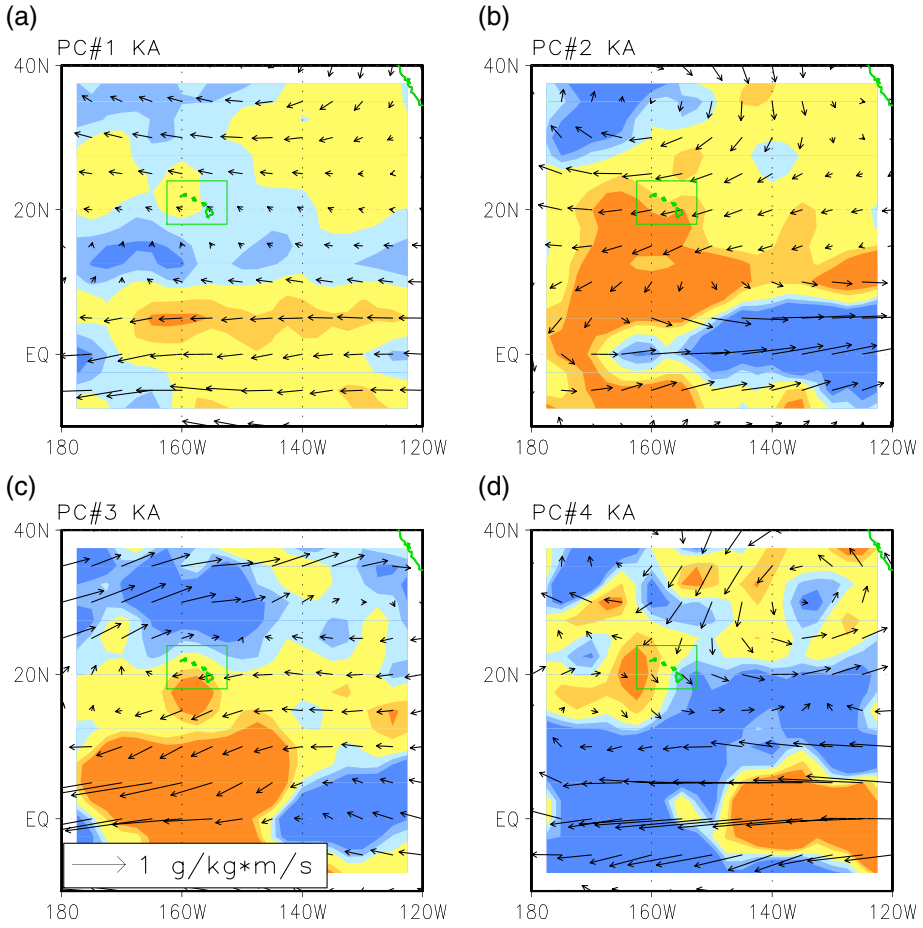


**Figure 8.** Same as Figure 7 but for the island of Kaua'i during the wet season.

The regression coefficients were interpolated with ordinary kriging for each of the four island groups. Maps are shown for the PC 1 time series (Figure 9a) and PC 4 time series (Figure 9b). The regression pattern analysis demonstrates two important connections between large-scale climate and local rainfall. First, we find in the regression pattern signatures of ENSO (and PNA), the primary drivers for rainfall variability in Hawai'i during the wet season. Typical El Niño (La Niña) years exhibit a uniform sign in the anomalies with below (above) average wet-season rainfall across the Hawaiian Islands (Figure 9a). The regression between PC 4 and the station rainfall anomalies, on the other hand, shows a dipole pattern between the dry leeward areas of the islands and the wet windward sides (Figure 9b). We will discuss this mode further in section 4.

### 3.3. Projected Future Changes

The statistical downscaling of the CMIP5 general circulation models was done in a multimodel ensemble mode with equal weights given to the 32 available models. We used the "historical" simulations and future scenarios RCP4.5 and RCP8.5 (2006–2100). The process steps are similar to the downscaling of the reanalysis data. In order to avoid model biases, we use the modeled present-day (1975–2005) climatology to standardize the resulting predictor time series. The simulated future changes in the predictors are measured relative to their present-day mean states.

To put the temporal changes of the predictor information into perspective, we show in Figure 10 how the 30 year averages in the predictor time series evolve in the historical and future scenario simulations; Hawai'i Island is shown as an example, but similar results are obtained for the other islands. The climate change signal of the multimodel ensemble projects mostly on the circulation anomaly pattern associated with the first and fourth PCA modes, which were used to compress the information from the stations' composite

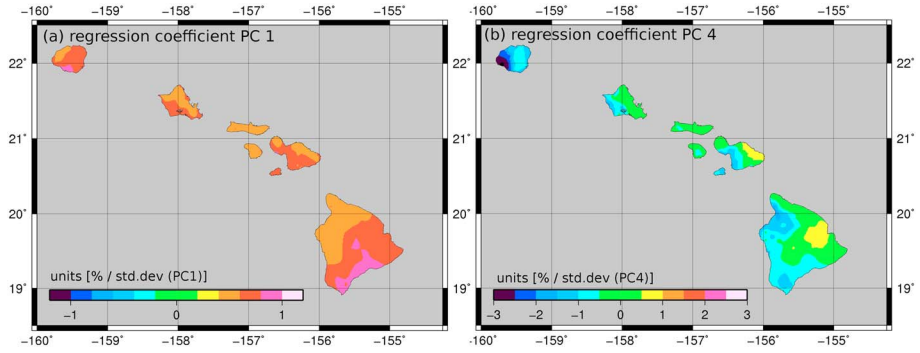


**Figure 9.** Maps of interpolated regression coefficients associated with the first and fourth PC time series for the wet season. (a) The leading mode shows a uniform pattern with small regional variations. (b) A dipole pattern is characterizing features of the regression pattern with PC 4.

analyses. This analysis indicates that the majority of the models project a continuous trend in the circulation anomalies from the 20th into the 21st century. Whereas the anomalies are small in the 20th century, the future changes are projected to grow in amplitude. In particular, the circulation changes resemble the anomaly pattern associated with the fourth mode and the first mode of the PCA (see circulation anomalies shown in Figures 4d, 5d, 7d, and 8d). The ensemble member spread increases with increasing signal amplitude, but the majority of the models agree at least in their sign. For PC 1 and PC 4, more than 75% of the models show negative and positive anomalies, respectively, in the future (see thick bars in Figure 10).

Using the regression coefficients, the temporal changes in the four-predictor time series are translated to rainfall anomalies at each station. For each of the 32 CMIP5 models, we estimated the percentage rainfall changes at all stations. The geographic map of the point-estimated changes clearly shows regional features that would not be directly available from the coarse-resolution CMIP5 model output. Stations on the wet sides of Hawai'i Island and Maui, for example, show neutral or positive rainfall anomalies for the future scenarios, and strong negative anomalies are seen in the dry regions on the leeward sides (Figures 11 and 12). The future rainfall anomalies are essentially a linear superposition of the regression coefficients associated with PC 1 and PC 4. An "ENSO-related" climate change component is represented by PC 1 and leads to an island-wide rainfall decrease, and PC 4 represents zonal shifts in the subtropical high or its westward extension and modifies the contrast between the wet and dry sides on the islands. We note that this enhanced or reduced wet-dry contrast in Hawai'i is a feature of the wet season. This mode of variability was not detected during the dry-season months.

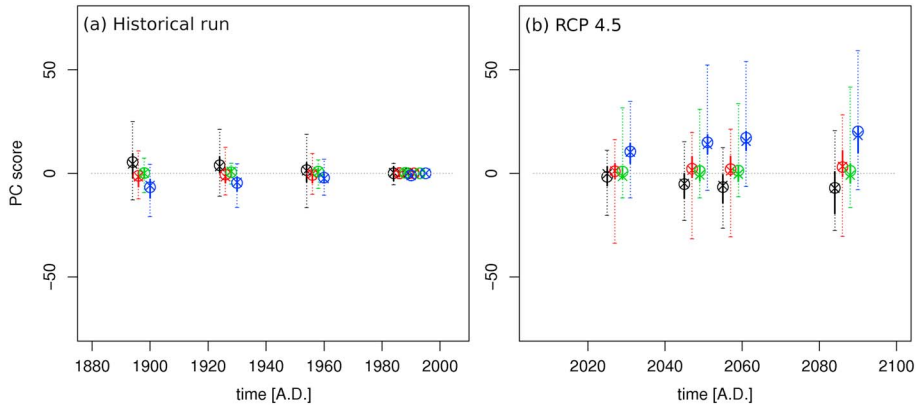


**Figure 10.** Wet-season time evolution of the PC time series for the island HA. Thirty year time averages of the PC time series were calculated from the 32-member multimodel ensemble using the CMIP5 historical and RCP4.5 scenarios. Colors highlight PC 1 (black), PC 2 (red), PC 3 (green), and PC 4 (blue). The ensemble statistics are shown: 30 year ensemble mean (circles), median (crosses), minimum-maximum range (dotted thin bars), and the 25%–75% quantile range (thick vertical bars). Note the continuous trend from the historical simulations to the future scenario in PC 1 and PC 4.

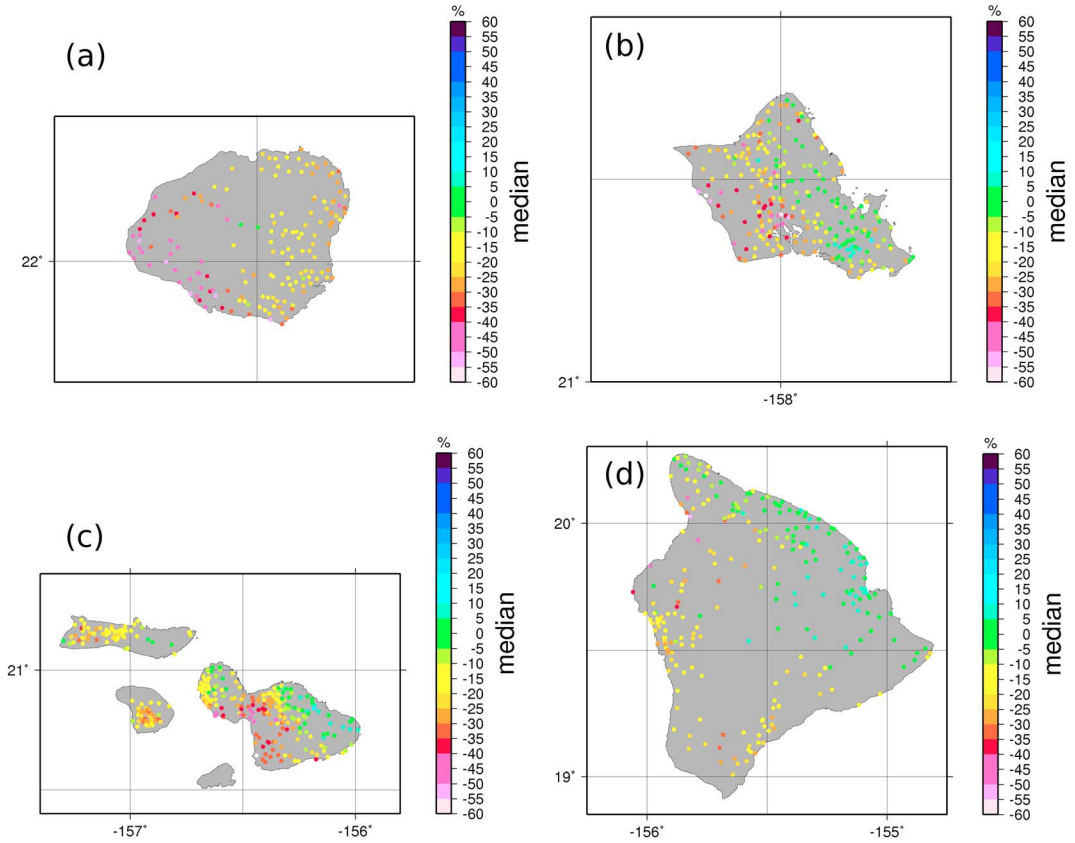


**Figure 11.** Statistical downscaling results of the 32-model CMIP5 ensemble for the moderate warming scenario RCP4.5. Shown are the stations' multimodel ensemble medians for wet season averaged over the period 2041–2071.

One of our priorities was to extend the spatial representation of the point station estimates. Whereas our statistical downscaling results are obtained at irregularly distributed point locations, geospatial methods were used to interpolate the downscaling results onto a regular grid. We have applied ordinary kriging for the four island regions with 0.5 min resolution. The resulting maps for the RCP4.5 and RCP8.5 scenarios are shown in Figure 13. The interpolated maps show clearly that the windward facing regions are expected to maintain or to slightly increase their wet-season rainfall. Other parts of the Hawaiian Islands, however, are projected to experience a continued trend toward lower wet-season precipitation.

The same statistical downscaling technique has been applied to the dry-season rainfall to illustrate that wet and dry seasons are under different climatic controls. Overall the dipole pattern in the projected changes is less pronounced during summer seasons, and only O'ahu appears to have contrasts between the wet and dry sides of the island similar to that projected for the wet season. Given the low cross-validation skill, it is not surprising that Kaua'i shows near-neutral conditions. Maui and Hawai'i Island are projected to have dryer conditions in most areas, including the high-precipitation sides along the windward slopes of the mountains.

## 4. Discussion

In this section, we provide a critical reflection on the implicit assumptions in our statistical downscaling method. We start with the general problem of the stationarity assumption in statistical downscaling methods. The last part of this section is devoted to the physical interpretation of the statistically derived changes in local rainfall.

### 4.1. Stationarity of the Rainfall-Circulation Relationships

An implicit, underlying assumption in this and other statistical downscaling methods—we are not aware of any truly nonstationary statistical downscaling method at this time—is deeply rooted in the scientific method of empiricism: that is, the statistical relationship established from past experiences is expected to describe

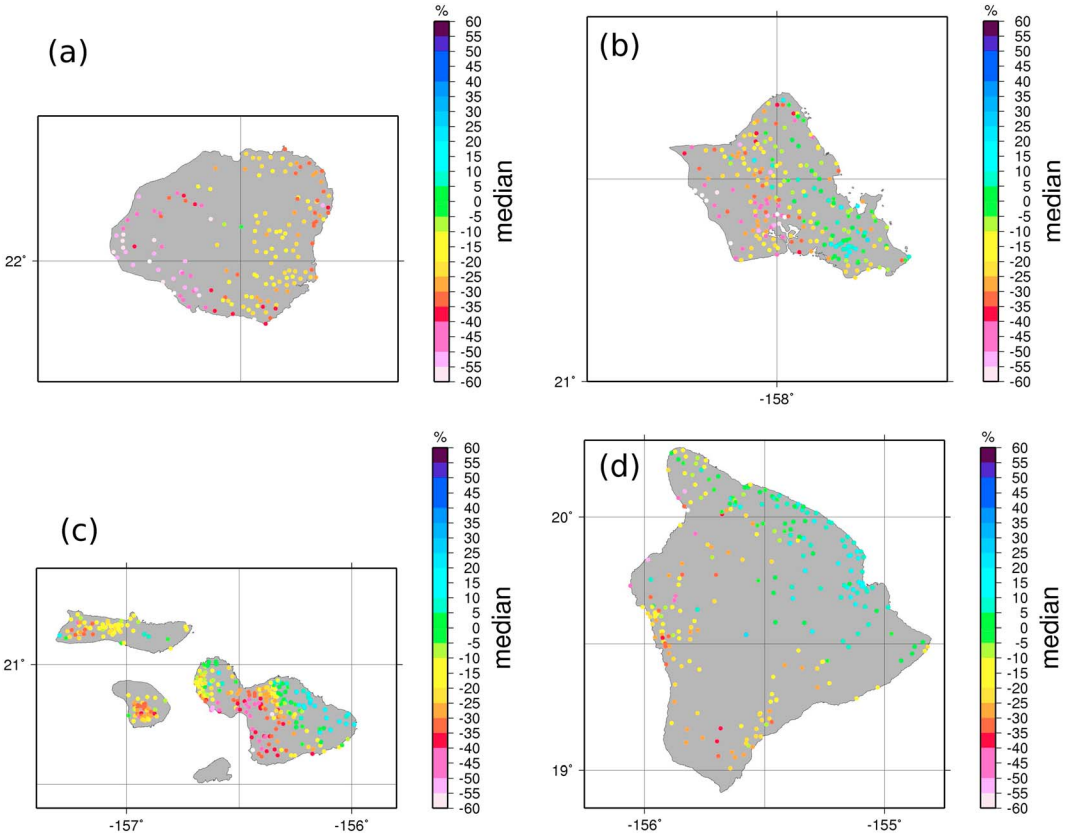


**Figure 12.** Same as in Figure 11 but for the more severe warming scenario RCP8.5 (wet season 2041–2071).

past and future processes with similar levels of uncertainty and to the degree possible untainted by any systematic biases. Our downscaling method relies on information from the variable covariances to form the composite patterns and multiple linear regression models. Given the complexity of the rain formation processes in Hawai'i that we described in section 1, it is possible that changes in the flow, vertical stability, or moisture content are capable of changing the fundamental mechanisms involved in the orographically induced rainfall. In such a case, we argue that our statistical downscaling should still give reasonable results in the moderate warming scenarios for the near future. The temperature changes over Hawai'i are expected to shift the daily mean temperatures to levels that are currently daily maximum values by the end of the century [*Lauer et al.*, 2013]. Furthermore, interannual temperature variability has influenced Hawai'i over the past years and decades [*Giambelluca et al.*, 2008; *Diaz et al.*, 2011; *Diaz and Giambelluca*, 2012]. Yet, no systematic and profound changes in the rain formation processes have been reported for trade wind regimes, land-sea breezes, or frontal systems. Thus, we argue that sudden nonlinear shifts in the rainfall pattern are unlikely to destroy the climatological relationships at least in the early part of the 21st century. This inductive inference is susceptible to a logical fallacy in which we might misinterpret "absence of evidence" as "evidence of absence." But without a priori theoretical knowledge of the existence of "tipping points," we have no reason to speculate if and when such a critical transition in the rainfall pattern may take place.

Nevertheless, if we assume that some statistical relationships would break down, it is worth exploring how nonstationarity could bias our results. Key to the downscaling was the formation of composite pattern upon which the climate models are projected. Changes in the teleconnection pattern have been reported for the ENSO-rainfall teleconnection pattern under future warming in the CMIP5 multimodel ensemble [*Bonfils and Santer*, 2010]. Mathematically, teleconnection patterns are vectors in a higher-dimensional space. They can change their strength (amplitude of the pattern), or change their spatial structure, or in worst case change their sign completely. If only the amplitude of our composite pattern was changed, it would not affect the vector projection result itself (due to normalization to unit length in the vector

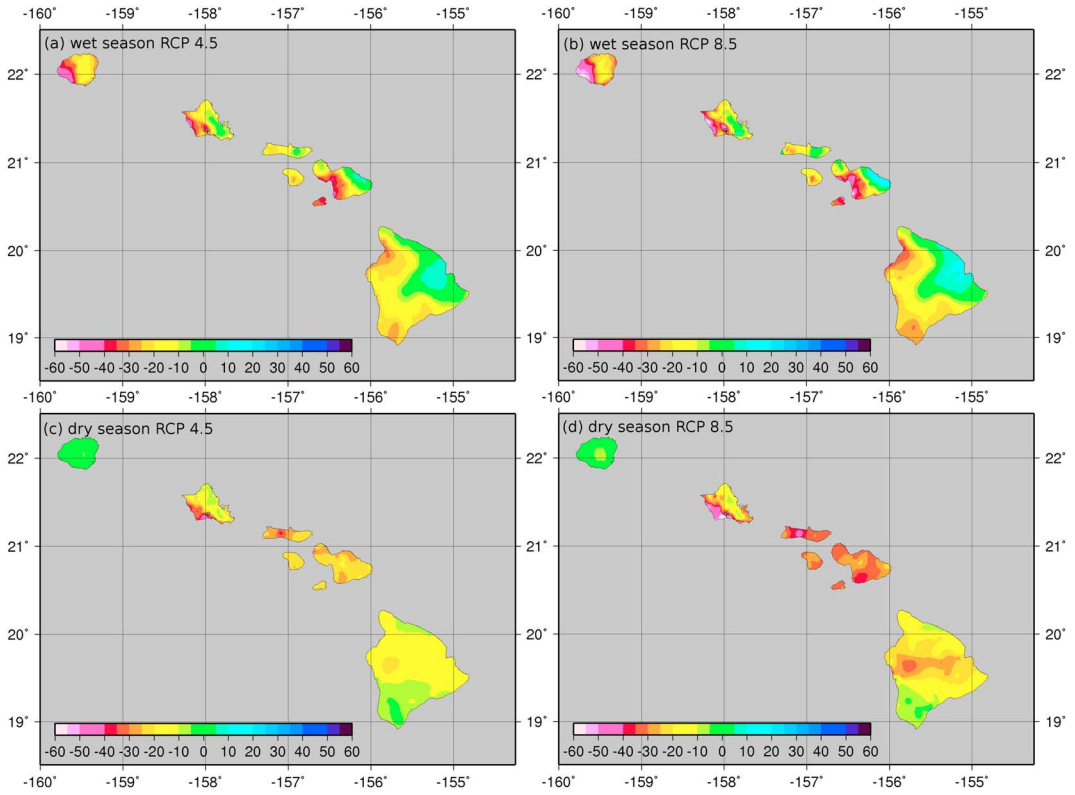


**Figure 13.** Interpolated maps of the statistically downscaled rainfall scenarios RCP4.5 and RCP8.5 for the period 2041–2071 (31 year time mean). Shown is the ensemble median result from 32 members from CMIP5. Units are given in percent.

projection), but it would cause a bias in the amplitude of the projected rainfall changes through the subsequent multiple linear regression model.

If on the other hand the vector changed its direction, this would contribute two types of errors to the rainfall downscaling. First, the change in the direction leads to a scaling bias (due to normalization to unit length in the vector projection), and second, a new orthogonal direction emerged in the large-scale circulation with influence on the rainfall anomalies. The latter is unaccounted for in the statistical downscaling model (unless this pattern change is projecting onto one of the other modes that are used as projection vectors). In either case, our defined static projection pattern cannot capture the true rainfall dependence any longer.

How large the individual biases could become in future would further depend on the pattern of the projected circulation changes—even if we had knowledge of the future teleconnection pattern (see Figure S2). Whether changes in rainfall amplitudes presented may be overestimated or underestimated is not immediately clear. In the worst case, our stationarity assumption could lead to misleading signs in the projected rainfall changes. The risk is considered low, given the fact that we include physically motivated predictor variables such as moisture transport and vertical stability. It has been argued that inclusion of precipitation and moisture-related predictor variables can reduce the risk of the nonstationarity problem in statistical downscaling [*Diaz et al.*, 2001; *Meehl and Teng*, 2007; *Sterl et al.*, 2007; *Kug et al.*, 2009; *Herceg Bulić et al.*, 2011; *Kwon et al.*, 2013; *Stevenson*, 2012; *Coats et al.*, 2013; *Zhou et al.*, 2014], but this assumption may miss some theoretical foundations, too [see also *Smith et al.*, 2014].

In order to test the stability of the teleconnection between large-scale variables and precipitation over the Hawaiian Islands, we analyzed the CMIP5 models. For each model the composite patterns were estimated in the historical runs and the RCP4.5 and RCP8.5 in 30 year time windows. The average of the modeled wet-season precipitation was used to form high and low precipitation composites (similar to the actual statistical downscaling method) and calculate the difference between high and low composites. Taking the historical scenario years (1975–2005) as the reference composite pattern, we then compared the future composites in

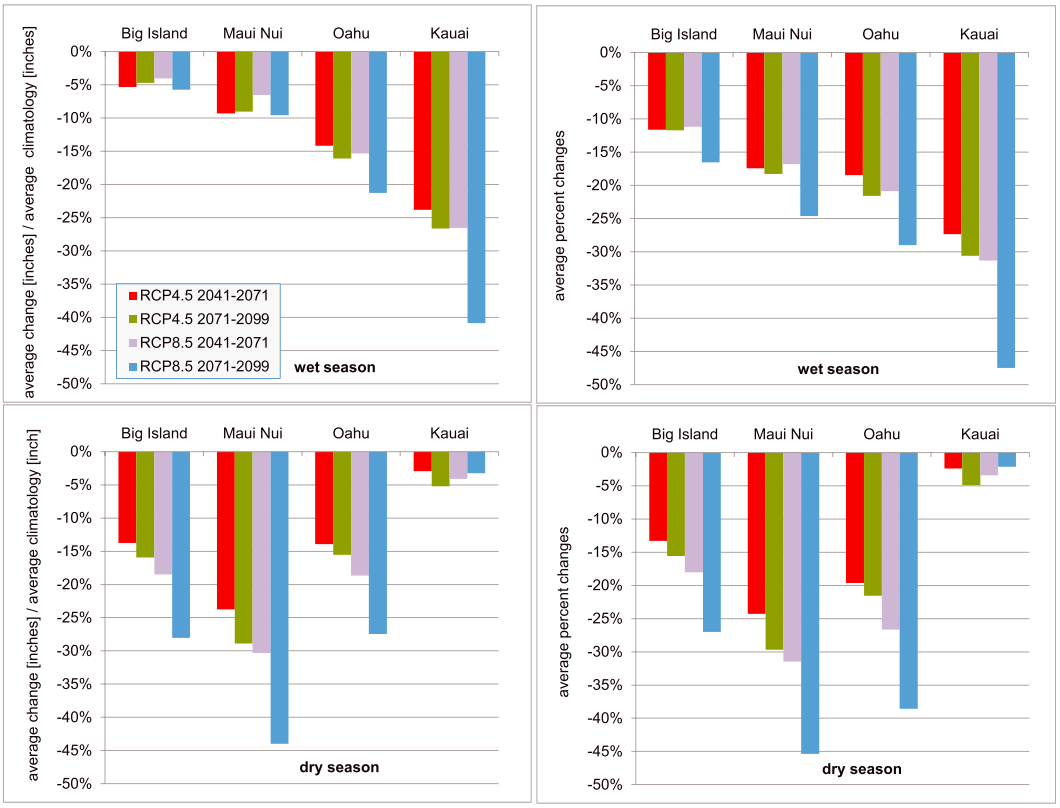


**Figure 14.** Summary statistics for the four islands groups. The top charts show the percentage changes averaged over the islands for the wet season (using interpolated maps). Bottom row shows the statistic for the dry season. Each island has four scenarios (RCP4.5 and RCP8.5 for the middle and late 21st century; see color legend). Right figures present for comparison the area-averaged precipitation anomalies when averaging the percentage changes (as shown in Figure 13) directly. Left figures show for comparison area-averaged precipitation changes expressed in percent of the island-average seasonal rainfall climatology from the Rainfall Atlas of Hawai'i [*Giambelluca et al*., 2013]. Note that for that purpose, we first converted the local percentage anomalies into absolute anomalies (in units of mm).

their spatial correlation and spatial standard deviation [*Taylor*, 2001]. The results for the composite pattern in the 500 hPa geopotential height fields are summarized in the Taylor diagram in Figure S3. It can be seen that the multimodel ensemble has a wide range of variability in the composite pattern. This is partly attributed to sampling uncertainty, since the historical runs already show large a spread in the amplitude and correlation values when the sampling window is changed using different years between years 1955 and 2005.

Compared with the historical samples, the future projections (red and orange symbols) slightly drift into systematic lower spatial correlation sectors but with a slight systematic increase in the range of standard deviations. Similar results have been obtained when using the specific humidity around Hawai'i as the compositing information. These results indicate that the current choice of the spatial domain includes areas with little robust information for Hawai'i's regional rainfall. The optimal domain size demands further investigations [*Timm and Diaz*, 2009; *Norton et al*., 2011]. For example, *Elison Timm et al*. [2013] restricted the spatial composite pattern to statistically significant subregions. We see in the deployment of pattern matching statistics a potential way to objectively find the most robust teleconnection pattern.

Although these results may indicate evidence against the nonstationarity assumption of our particular method, a deeper investigation of the stability of teleconnection pattern over the North Pacific is suggested as a future research direction.

Whether the true covariance relationship between the local rainfall and the large-scale circulation behaves similar to the CMIP5-based teleconnection analysis cannot be answered until high-resolution dynamical downscaling methods will allow for systematic tests. At present, it remains a fundamental challenge to support the stationarity assumption for future climate scenarios [*Wilby*, 1997; *Charles et al*., 1999; *Fowler et al*.,

2005; *Vrac et al*., 2007; *Christensen et al*., 2008; *Raje and Mujumdar*, 2010; *Maraun*, 2012; *Hewitson et al*., 2013]. The latest IPCC report from working group 1 acknowledges that statistical downscaling relies on the "stationarity hypothesis," without giving any comprehensive discussion of its inherent problems or possible solutions [*IPCC*, 2013, Chapter, 9.6].

Observational evidence for nonstationarity on decadal or longer time scales is difficult to assess, given the relatively short observational data period. Therefore, we lack empirical support for determining if or when we can expect a breakdown of the historical relationships, which could undermine the statistical downscaling methods. Efforts toward developing more rigorous tests of stationarity are in development [*Schmith*, 2008; *Gutiérrez et al*., 2013; *Hertig and Jacobeit*, 2013] but remain insufficient. Other critical tests may be needed to improve the choice of the statistical model and its parameters [*Estrada et al*., 2013], and rigorous cross-validation methods can help to assess skills and biases of the statistical models. Alternatively, one could pursue a cross-validation strategy using surrogate data from dynamically downscaled climate scenarios. Recent attempts to test statistical model performance under present-day and future conditions within a regional climate model appear to be the most promising efforts to answer that question (Keith W. Dixon, presentation at the AMS 25th Conference on Climate Variability and Change, Austin Texas, 5–10 January 2013; https://ams.confex.com/ams/93Annual/webprogram/Paper221738.html).

### 4.2. Physical Interpretation of the Statistical Results

The circulation anomalies in the CMIP5 models show a trend toward stronger Aleutian Lows and stabilization of the atmosphere in the subtropics. The statistical downscaling method used here identifies this category of circulation anomalies as an El Niño-like condition/positive PNA pattern and thus associates drier than average conditions with this projected circulation anomaly. Associated with this mode is a poleward shift in wintertime midlatitude storm tracks near Hawai'i, resulting in fewer cold fronts, Kona lows, and other cyclonic disturbances during the wet season, which produce rainfall on both leeward and windward sides of the islands. However, the ensemble median circulation anomalies that develop through the 21st century project even more strongly on a secondary mode that is uncorrelated with the typical ENSO/PNA signature. These circulation anomalies represent a zonal shift in the position or extension of the subtropical high or a systematic change in the positioning and eastward migration of extratropical troughs. In the past, this type of large-scale circulation anomaly is associated with a rainfall pattern that enhances the rainfall contrast between the wet windward and dry leeward regions (on Maui, O'ahu, and Hawai'i) and that generally has its greatest effect in areas where rainfall amounts are controlled by cyclonic disturbances. It should be noted that the Hawaiian Islands have experienced a number of years with station rainfall anomalies showing a bimodal distribution. For example, the 1994–1995 wet season exhibits a dipole pattern in the observed rainfall anomalies with strong negative anomalies in the leeward sides and slightly enhanced or average rainfall in the windward areas. Two years later, the reverse pattern was observed in Hawai'i. This mode of variability was identified in earlier studies [*Lyons*, 1982].

It appears that lower-ranked climate modes (PCA modes with less explained variability) are important for projecting regional climate change [*Bond et al*., 2003; *Keeley et al*., 2008]. In our downscaled projections, the subtropical zonal dipole pattern constitutes a robust feature in multimodel ensemble projections. Although the dynamical reasons behind these circulation shifts are currently not well understood, an interplay between the position and extension of the Asian jet and subtropical cyclone activity and blocking events might play an important role in the central and eastern Pacific [*Chu*, 1995; *Huang et al*., 2004; *Otkin and Martin*, 2004b; *Jayawardena et al*., 2012]. Zonally aligned dipole-like circulation anomaly patterns can be found in various mode decompositions of the atmospheric circulation [*Wallace and Gutzler*, 1981; *Barnston and Livezey*, 1987; *Johnson and Feldstein*, 2010]. The combined effects from these circulation changes indicate that the largest rainfall decreases are expected in the dry regions, with neutral or positive anomalies projected for the wet windward sides of the islands. This spatial pattern was not resolved in our earlier study (TD09).

Future changes in circulation anomalies suggest that the dry season will become dryer. However, our confidence in the spatial pattern and in the amplitudes of the projected changes is lower than for the wet season. Lower confidence in the dry-season results is mainly due to the nature of rainfall-generating processes during the summer months. With the exception of the trade wind dominated rainfall in windward areas, summer rainfall is limited to a small number of significant weather events during the season. The passing of strong fronts and the occurrence of Kona lows are limited to the wet season [*Daingerfield*, 1921;

*Sanderson*, 1993; *Otkin and Martin*, 2004a; *Caruso and Businger*, 2006]. During the summer season atmospheric disturbances are of smaller scale and less frequent, leaving thus a smaller imprint in the seasonal mean circulation anomalies than winter disturbances. Thus, the effects of increases in tropical storms in the central Pacific [*Murakami et al.*, 2013] are not accounted for in the statistical model. It is clear that the seasonal mean circulation anomalies, which are used as linear predictors for local rainfall, cannot provide sufficient statistical information to obtain reliable rainfall estimates. We note, however, that nonlinear methods could improve the dry-season downscaling skill [e.g., *Norton et al.*, 2011].

In comparison with our earlier study (TD09), the magnitude of the precipitation changes projected here are larger on average. In the analysis presented here, we project rainfall anomalies in the ensemble median of severe magnitude by 2040–2070. In many drought-prone regions the future projections suggest reductions by more than 50%, but the absolute values must be considered with caution. We note that the concept of the statistical downscaling is building on the assumption that future climate states are shifting the frequency of weather pattern and circulation anomalies. Changes in the relationship between circulation anomalies and regional rainfall could ultimately invalidate this assumption. Our results are understood as a linear approach to project "small" or moderate changes. Nonlinear processes in the hydrological cycle response are not captured in this model. Independent downscaling results with a dynamical regional model (C. Zhang and K. Hamilton, personal communication, Honolulu, Hawaii, 2014) show qualitatively similar spatial patterns, but the amplitudes of the changes in dry areas are smaller, and the positive anomalies have larger values in the regional model simulation. In the dynamical model simulation, the orographic effects on the moisture convergence seem to dictate the regional response in the rainfall in both seasons. It should be noted that the applied pseudoglobal warming method does not account for changes in the weather pattern and their frequency.

## 5. Summary

A linear statistical downscaling approach was applied to the ensemble median of 32 CMIP5 model simulations of the present-day and modeled future climate scenarios. The resulting statistical point estimates were interpolated to produce maps of expected rainfall changes for the main Hawaiian Islands. Given past observations of relationships between seasonally averaged circulation anomalies and local rainfall anomalies, the information from the CMIP5 models was transformed into future rainfall anomalies. Under an assumption of stationarity in the relationship between local rainfall and large-scale climate, the future scenario for the Hawaiian Islands projects, on average, a decrease in the rainfall (Figure 14) and, hence, reduced availability of freshwater resources. We estimate a decrease in wet-season rainfall in most areas of the islands with the exception of the trade wind dominated wet regions along and above the eastern slopes of the mountains, where slight increases in the rainfall can be expected based on the projected CMIP5 circulation changes.

Despite all the limitations of the statistical downscaling method, it is estimated that a trend toward drier than normal conditions is likely to affect the climatically dry regions of the Hawaiian Islands during both seasons. The wet sides of the islands are likely to see small increases in the average wet-season rainfall amounts.

**Acknowledgments**

The project described in this publication was supported by grant/cooperative agreement 12200-A-J-024/ F10AC00077 from the DOI FWS Pacific Island Climate Change Cooperative (PICCC) and G12AC20502 from the USGS Pacific Island Climate Science Center (PICSC). Its contents are solely the responsibility of the authors and do not necessarily represent the official views of the USGS. We acknowledge the World Climate Research Programme's Working Group on Coupled Modelling, which is responsible for CMIP, and we thank the climate modeling groups (listed in Table 2 of this paper) for providing their model output. For CMIP the U.S. Department of Energy's Program for Climate Model Diagnosis and Intercomparison provides coordinating support and led development of software infrastructure in partnership with the Global Organization for Earth System Science Portals. The authors thank the three anonymous reviewers for their constructive criticisms. Data policy: The data sets with the downscaling results (Figures 2 and 11-13) and additional supporting data and metadata will be made available through the Asia-Pacific Data-Research Center (APDRC, http://apdrc.soest.hawaii.edu/).

## References

Barnston, A. G., and R. E. Livezey (1987), Classification, seasonality and persistence of low-frequency atmospheric circulation patterns, *Mon. Weather Rev.*, *115*(6), 1083–1126, doi:10.1175/1520-0493(1987)115<1083:CSAPOL>2.0.CO;2.

Benestad, R. E. (2001), A comparison between two empirical downscaling strategies, *Int. J. Climatol.*, *21*(13), 1645–1668, doi:10.1002/joc.703.

Bond, N. A., J. E. Overland, M. Spillane, and P. Stabeno (2003), Recent shifts in the state of the North Pacific, *Geophys. Res. Lett.*, *30*(23), 2183, doi:10.1029/2003GL018597.

Bonfils, C., and B. D. Santer (2010), Investigating the possibility of a human component in various Pacific decadal oscillation indices, *Clim. Dyn.*, *37*(7–8), 1457–1468, doi:10.1007/s00382-010-0920-1.

Brands, S., J. M. Gutiérrez, S. Herrera, and A. S. Cofiño (2012), On the use of reanalysis data for downscaling, *J. Clim.*, *25*(7), 2517–2526, doi:10.1175/JCLI-D-11-00251.1.

Caruso, S. J., and S. Businger (2006), Subtropical cyclogenesis over the Central North Pacific*, *Weather Forecasting*, *21*(2), 193–205, doi:10.1175/WAF914.1.

Charles, S., B. Bates, P. Whetton, and J. Hughes (1999), Validation of downscaling models for changed climate conditions: Case study of southwestern Australia, *Clim. Res.*, *12*, 1–14, doi:10.3354/cr012001.

Chen, Y.-L., and A. J. Nash (1994), Diurnal variation of surface airflow and rainfall frequencies on the island of Hawaii, *Mon. Weather Rev.*, *122*(1), 34–56, doi:10.1175/1520-0493(1994)122<0034:DVOSAA>2.0.CO;2.

Christensen, J. H., F. Boberg, O. B. Christensen, and P. Lucas-Picher (2008), On the need for bias correction of regional climate change projections of temperature and precipitation, *Geophys. Res. Lett.*, *35*, L20709, doi:10.1029/2008GL035694.

Chu, P.-S. (1995), Hawaii rainfall anomalies and El Niño, *J. Clim.*, *8*(6), 1697–1703, doi:10.1175/1520-0442(1995)008<1697:HRAAEN>2.0.CO;2.

Chu, P.-S., and H. Chen (2005), Interannual and interdecadal rainfall variations in the Hawaiian islands, *J. Clim.*, *18*(22), 4796–4813, doi:10.1175/JCLI3578.1.
Coats, S., J. E. Smerdon, B. I. Cook, and R. Seager (2013), Stationarity of the tropical Pacific teleconnection to North America in CMIP5/PMIP3 model simulations, *Geophys. Res. Lett.*, *40*, 4927–4932, doi:10.1002/grl.50938.
Daingerfield, L. H. (1921), Kona storms, *Mon. Weather Rev.*, *49*(6), 327–329, doi:10.1175/1520-0493(1921)49<327:KS>2.0.CO;2.
Diaz, H. F., and T. W. Giambelluca (2012), Changes in atmospheric circulation patterns associated with high and low rainfall regimes in the Hawaiian Islands region on multiple time scales, *Global Planet. Change*, *98–99*, 97–108, doi:10.1016/j.gloplacha.2012.08.011.
Diaz, H. F., M. P. Hoerling, and J. K. Eischeid (2001), ENSO variability, teleconnections and climate change, *Int. J. Climatol.*, *21*(15), 1845–1862, doi:10.1002/joc.631.
Diaz, H. F., T. W. Giambelluca, and J. K. Eischeid (2011), Changes in the vertical profiles of mean temperature and humidity in the Hawaiian Islands, *Global Planet. Change*, *77*(1–2), 21–25, doi:10.1016/j.gloplacha.2011.02.007.
Elison Timm, O., H. F. Diaz, T. W. Giambelluca, and M. Takahashi (2011), Projection of changes in the frequency of heavy rain events over Hawaii based on leading Pacific climate modes, *J. Geophys. Res.*, *116*, D04109, doi:10.1029/2010JD014923.
Elison Timm, O., M. Takahashi, T. W. Giambelluca, and H. F. Diaz (2013), On the relation between large-scale circulation pattern and heavy rain events over the Hawaiian Islands: Recent trends and future changes, *J. Geophys. Res. Atmos.*, *118*, 4129–4141, doi:10.1002/jgrd.50314.
Estrada, F., V. M. Guerrero, C. Gay-García, and B. Martínez-López (2013), A cautionary note on automated statistical downscaling methods for climate change, *Clim. Change*, *120*(1–2), 263–276, doi:10.1007/s10584-013-0791-7.
Fowler, H. J., C. G. Kilsby, P. E. O'Connell, and A. Burton (2005), A weather-type conditioned multi-site stochastic rainfall model for the generation of scenarios of climatic variability and change, *J. Hydrol.*, *308*(1–4), 50–66, doi:10.1016/j.jhydrol.2004.10.021.
Giambelluca, T. W., H. F. Diaz, and M. S. A. Luke (2008), Secular temperature changes in Hawai'i, *Geophys. Res. Lett.*, *35*, L12702, doi:10.1029/2008GL034377.
Giambelluca, T. W., Q. Chen, A. G. Frazier, J. P. Price, Y.-L. Chen, P.-S. Chu, J. K. Eischeid, and D. M. Delparte (2013), Online Rainfall Atlas of Hawai'i, *Bull. Am. Meteorol. Soc.*, *94*(3), 313–316, doi:10.1175/BAMS-D-11-00228.1.
Gutiérrez, J. M., D. San-Martín, S. Brands, R. Manzanas, and S. Herrera (2013), Reassessing statistical downscaling techniques for their robust application under climate change conditions, *J. Clim.*, *26*(1), 171–188, doi:10.1175/JCLI-D-11-00687.1.
Hartley, T. M., and Y.-L. Chen (2010), Characteristics of summer trade wind rainfall over Oahu, *Weather Forecasting*, *25*(6), 1797–1815, doi:10.1175/2010WAF2222328.1.
Herceg Bulić, I., Č. Branković, and F. Kucharski (2011), Winter ENSO teleconnections in a warmer climate, *Clim. Dyn.*, *38*(7–8), 1593–1613, doi:10.1007/s00382-010-0987-8.
Hertig, E., and J. Jacobeit (2013), A novel approach to statistical downscaling considering nonstationarities: Application to daily precipitation in the Mediterranean area, *J. Geophys. Res. Atmos.*, *118*, 520–533, doi:10.1002/jgrd.50112.
Hewitson, B. C., J. Daron, R. G. Crane, M. F. Zermoglio, and C. Jack (2013), Interrogating empirical-statistical downscaling, *Clim. Change*, *122*(4), 539–554, doi:10.1007/s10584-013-1021-z.
Hobbelen, P. H. F., M. D. Samuel, D. A. LaPointe, and C. T. Atkinson (2012), Modeling future conservation of Hawaiian honeycreepers by mosquito management and translocation of disease-tolerant Amakihi, *PLoS One*, *7*(11), e49594, doi:10.1371/journal.pone.0049594.
Huang, F., F. Zhou, and M. H. England (2004), Atmospheric circulation associated with anomalous variations in North Pacific wintertime blocking, *Mon. Weather Rev.*, *132*(5), 1049–1064, doi:10.1175/1520-0493(2004)132<1049:ACAWAV>2.0.CO;2.
Intergovernmental Panel on Climate Change (IPCC) (2007), Contribution of working group I to the fourth assessment report of the Intergovernmental Panel on Climate Change, in *Climate Change 2007: The Physical Science Basis*, edited by S. Solomon et al., Cambridge Univ. Press, Cambridge, U. K., and New York.
Intergovernmental Panel on Climate Change (IPCC) (2013), Contribution of working group I to the fifth assessment report of the Intergovernmental Panel on Climate Change, in *Climate Change 2013: The Physical Science Basis*, edited by T. F. Stocker et al., Cambridge Univ. Press, Cambridge, U. K., and New York.
Jayawardena, I. M. S., Y.-L. Chen, A. J. Nash, and K. Kodama (2012), A comparison of three prolonged periods of heavy rainfall over the Hawaiian Islands, *J. Appl. Meteorol. Climatol.*, *51*(4), 722–744, doi:10.1175/JAMC-D-11-0133.1.
Johnson, N. C., and S. B. Feldstein (2010), The continuum of North Pacific sea level pressure patterns: Intraseasonal, interannual, and interdecadal variability, *J. Clim.*, *23*(4), 851–867, doi:10.1175/2009JCLI3099.1.
Judge, S. W., J. M. Gaudioso, P. M. Gorresen, and R. J. Camp (2012), Reoccurrence of 'Oma'o in Leeward Woodland habitat and their distribution in alpine habitat on Hawai'i island, *Wilson J. Ornithol.*, *124*(4), 675–681.
Keeley, S. P. E., M. Collins, and A. J. Thorpe (2008), Northern Hemisphere winter atmospheric climate: Modes of natural variability and climate change, *Clim. Dyn.*, *31*(2–3), 195–211, doi:10.1007/s00382-007-0346-6.
Kirshbaum, D. J., and R. B. Smith (2009), Orographic precipitation in the tropics: Large-Eddy simulations and theory, *J. Atmos. Sci.*, *66*(9), 2559–2578, doi:10.1175/2009JAS2990.1.
Kodama, K., and G. M. Barnes (1997), Heavy rain events over the south-facing slopes of Hawaii: Attendant conditions, *Weather Forecasting*, *12*(2), 347–367, doi:10.1175/1520-0434(1997)012<0347:HREOTS>2.0.CO;2.
Kug, J.-S., S.-I. An, Y.-G. Ham, and I.-S. Kang (2009), Changes in El Niño and La Niña teleconnections over North Pacific–America in the global warming simulations, *Theor. Appl. Climatol.*, *100*(3–4), 275–282, doi:10.1007/s00704-009-0183-0.
Kwon, M., S.-W. Yeh, Y.-G. Park, and Y.-K. Lee (2013), Changes in the linear relationship of ENSO-PDO under the global warming, *Int. J. Climatol.*, *33*(5), 1121–1128, doi:10.1002/joc.3497.
LaPointe, D. A., C. T. Atkinson, and M. D. Samuel (2012), Ecology and conservation biology of avian malaria, edited by R. S. Ostfeld and W. H. Schlesinger, *Ann. N.Y. Acad. Sci.*, *1249*, 211–226, doi:10.1111/j.1749-6632.2011.06431.x.
Lauer, A., C. Zhang, O. Elison-Timm, Y. Wang, and K. Hamilton (2013), Downscaling of climate change in the Hawaii region using CMIP5 results: On the choice of the forcing fields*, *J. Clim.*, *26*(24), 10,006–10,030, doi:10.1175/JCLI-D-13-00126.1.
Lavoie, R. L. (1967), The warm rain project in Hawaii, *Tellus*, *19*(3), 347, doi:10.1111/j.2153-3490.1967.tb01488.x.
Leopold, L. B. (1949), The interaction of trade wind and sea breeze, Hawaii, *J. Meteorol.*, *6*(5), 312–320, doi:10.1175/1520-0469(1949)006<0312:TIOTWA>2.0.CO;2.
Lyons, S. W. (1982), Empirical orthogonal function analysis of Hawaiian rainfall, *J. Appl. Meteorol.*, *21*(11), 1713–1729, doi:10.1175/1520-0450(1982)021<1713:EOFAOH>2.0.CO;2.
Maraun, D. (2012), Nonstationarities of regional climate model biases in European seasonal mean temperature and precipitation sums, *Geophys. Res. Lett.*, *39*, L06706, doi:10.1029/2012GL051210.
Maraun, D., et al. (2010), Precipitation downscaling under climate change: Recent developments to bridge the gap between dynamical models and the end user, *Rev. Geophys.*, *48*, RG3003, doi:10.1029/2009RG000314.

Mearns, L. O., W. Gutowski, R. Jones, R. Leung, S. McGinnis, A. Nunes, and Y. Qian (2009), A regional climate change assessment program for North America, *Eos Trans. AGU*, *90*(36), 311–312, doi:10.1029/2009EO360002.
Meehl, G. A., and H. Teng (2007), Multi-model changes in El Niño teleconnections over North America in a future warmer climate, *Clim. Dyn.*, *29*(7–8), 779–790, doi:10.1007/s00382-007-0268-3.
Murakami, H., B. Wang, T. Li, and A. Kitoh (2013), Projected increase in tropical cyclones near Hawaii, *Nat. Clim. Change*, *3*(8), 749–754, doi:10.1038/nclimate1890.
Norton, C. W., P.-S. Chu, and T. A. Schroeder (2011), Projecting changes in future heavy rainfall events for Oahu, Hawaii: A statistical downscaling approach, *J. Geophys. Res.*, *116*, D17110, doi:10.1029/2011JD015641.
Nullet, D., and M. Mcgranaghan (1988), Rainfall enhancement over the Hawaiian Islands, *J. Clim.*, *1*(8), 837–839, doi:10.1175/1520-0442(1988)001<0837:REOTHI>2.0.CO;2.
Otkin, J. A., and J. E. Martin (2004a), A synoptic climatology of the subtropical Kona storm, *Mon. Weather Rev.*, *132*(6), 1502–1517, doi:10.1175/1520-0493(2004)132<1502:ASCOTS>2.0.CO;2.
Otkin, J. A., and J. E. Martin (2004b), The large-scale modulation of subtropical cyclogenesis in the Central and Eastern Pacific Ocean, *Mon. Weather Rev.*, *132*(7), 1813–1828, doi:10.1175/1520-0493(2004)132<1813:TLMOSC>2.0.CO;2.
Power, S. B., F. Delage, R. Colman, and A. Moise (2012), Consensus on twenty-first-century rainfall projections in climate models more widespread than previously thought, *J. Clim.*, *25*(11), 3792–3809, doi:10.1175/JCLI-D-11-00354.1.
Raje, D., and P. P. Mujumdar (2010), Constraining uncertainty in regional hydrologic impacts of climate change: Nonstationarity in downscaling, *Water Resour. Res.*, *46*, W07543, doi:10.1029/2009WR008425.
Rasmussen, R. M., P. Smolarkiewicz, and J. Warner (1989), On the dynamics of Hawaiian cloud bands: Comparison of model results with observations and island climatology, *J. Atmos. Sci.*, *46*(11), 1589–1608, doi:10.1175/1520-0469(1989)046<1589:OTDOHC>2.0.CO;2.
Sanderson, M. (Ed.) (1993), *Prevailing Trade Winds: Weather and Climate in Hawai'i*, University of Hawaii Press, Honolulu.
Schmith, T. (2008), Stationarity of regression relationships: Application to empirical downscaling, *J. Clim.*, *21*(17), 4529–4537, doi:10.1175/2008JCLI1910.1.
Smith, M. J., P. I. Palmer, D. W. Purves, M. C. Vanderwel, V. Lyutsarev, B. Calderhead, L. N. Joppa, C. M. Bishop, and S. Emmott (2014), Changing how earth system modeling is done to provide more useful information for decision making, science, and society, *Bull. Am. Meteorol. Soc.*, *95*(9), 1453–1464, doi:10.1175/BAMS-D-13-00080.1.
Smith, R., and I. Barstad (2004), A linear theory of orographic precipitation, *J. Atmos. Sci.*, *61*, 1377–1391.
Smolarkiewicz, P. K., R. M. Rasmussen, and T. L. Clark (1988), On the dynamics of Hawaiian cloud bands: Island forcing, *J. Atmos. Sci.*, *45*(13), 1872–1905, doi:10.1175/1520-0469(1988)045<1872:OTDOHC>2.0.CO;2.
Sobel, A. H., C. D. Burleyson, and S. E. Yuter (2011), Rain on small tropical islands, *J. Geophys. Res.*, *116*, D08102, doi:10.1029/2010JD014695.
Sobie, S. R., and A. J. Weaver (2012), Downscaling of precipitation over Vancouver Island using a synoptic typing approach, *Atmos. Ocean*, *50*(2), 176–196, doi:10.1080/07055900.2011.641908.
Sterl, A., G. J. van Oldenborgh, W. Hazeleger, and G. Burgers (2007), On the robustness of ENSO teleconnections, *Clim. Dyn.*, *29*(5), 469–485, doi:10.1007/s00382-007-0251-z.
Stevenson, S. L. (2012), Significant changes to ENSO strength and impacts in the twenty-first century: Results from CMIP5, *Geophys. Res. Lett.*, *39*, L17703, doi:10.1029/2012GL052759.
Takahashi, T. (1977), A study of Hawaiian warm rain showers based on aircraft observation, *J. Atmos. Sci.*, *34*(11), 1773–1790, doi:10.1175/1520-0469(1977)034<1773:ASOHWR>2.0.CO;2.
Tanaka, K., M. W. Guidry, and N. Gruber (2013), Ecosystem responses of the subtropical Kaneohe Bay, Hawaii, to climate change: A nitrogen cycle modeling approach, *Aquat. Geochem.*, *19*(5–6), 569–590, doi:10.1007/s10498-013-9209-4.
Taylor, K. E. (2001), Summarizing multiple aspects of model performance in a single diagram, *J. Geophys. Res.*, *106*(D7), 7183–7192, doi:10.1029/2000JD900719.
Taylor, K. E., R. J. Stouffer, and G. A. Meehl (2012), An overview of CMIP5 and the experiment design, *Bull. Am. Meteorol. Soc.*, *93*(4), 485–498, doi:10.1175/BAMS-D-11-00094.1.
Thrasher, B., J. Xiong, W. Wang, F. Melton, A. Michaelis, and R. Nemani (2013), Downscaled climate projections suitable for resource management, *Eos Trans. AGU*, *94*(37), 321–323, doi:10.1002/2013EO370002.
Timm, O., and H. F. Diaz (2009), Synoptic-statistical approach to regional downscaling of IPCC twenty-first-century climate projections: Seasonal rainfall over the Hawaiian islands*, *J. Clim.*, *22*(16), 4261–4280, doi:10.1175/2009JCLI2833.1.
Vrac, M., M. L. Stein, K. Hayhoe, and X.-Z. Liang (2007), A general method for validating statistical downscaling methods under future climate change, *Geophys. Res. Lett.*, *34*, L18701, doi:10.1029/2007GL030295.
Wallace, J. M., and D. S. Gutzler (1981), Teleconnections in the geopotential height field during the Northern Hemisphere winter, *Mon. Weather Rev.*, *109*(4), 784–812, doi:10.1175/1520-0493(1981)109<0784:TITGHF>2.0.CO;2.
Wang, J., and X. Zhang (2008), Downscaling and projection of winter extreme daily precipitation over North America, *J. Clim.*, *21*(5), 923–937, doi:10.1175/2007JCLI1671.1.
Wilby, R. L. (1997), Non-stationarity in daily precipitation series: Implications for GCM down-scaling using atmospheric circulation indices, *Int. J. Climatol.*, *17*(4), 439–454, doi:10.1002/(SICI)1097-0088(19970330)17:4<439::AID-JOC145>3.0.CO;2-U.
Wilby, R. L., S. P. Charles, E. Zorita, B. Timbal, P. Whetton, and L. O. Mearns (2004), Guidelines for use of climate scenarios developed from statistical downscaling methods.
Wilks, D. S. (2006), *Statistical Methods in the Atmospheric Sciences*, 2nd ed., Elsevier, Amsterdam, Boston, Heidelberg, London.
Wuebbles, D. J., K. Kunkel, M. Wehner, and Z. Zobel (2014), Severe weather in United States under a changing climate, *Eos Trans. AGU*, *95*(18), 149–150.
Xie, S.-P., W. T. Liu, Q. Liu, and M. Nonaka (2001), Far-reaching effects of the Hawaiian Islands on the Pacific Ocean-atmosphere system, *Science*, *292*, 2057–2060, doi:10.1126/science.1059781.
Yang, Y., and Y.-L. Chen (2003), Circulations and rainfall on the lee side of the island of Hawaii during HaRP*, *Mon. Weather Rev.*, *131*(10), 2525–2542, doi:10.1175/1520-0493(2003)131<2525:CAROTL>2.0.CO;2.
Yang, Y., and Y.-L. Chen (2008), Effects of terrain heights and sizes on island-scale circulations and rainfall for the island of Hawaii during HaRP, *Mon. Weather Rev.*, *136*(1), 120–146, doi:10.1175/2007MWR1984.1.
Zhang, C., Y. Wang, A. Lauer, and K. Hamilton (2012), Configuration and evaluation of the WRF model for the study of Hawaiian regional climate, *Mon. Weather Rev.*, *140*(10), 3259–3277, doi:10.1175/MWR-D-11-00260.1.
Zhang, Y., Y.-L. Chen, and K. Kodama (2005), Validation of the coupled NCEP mesoscale spectral model and an advanced land surface model over the Hawaiian islands. Part II: A high wind event*, *Weather Forecasting*, *20*(6), 873–895, doi:10.1175/WAF892.1.
Zhou, Z.-Q., S.-P. Xie, X.-T. Zheng, Q. Liu, and H. Wang (2014), Global warming-induced changes in El Niño teleconnections over the North Pacific and North America, *J. Clim.*, doi:10.1175/JCLI-D-14-00254.1, in press.

Auxiliary Material

# Statistical Downscaling of Rainfall Changes in Hawai‘i based on the CMIP5 Global Model Projections

Oliver Elison Timm[1], Thomas W. Giambelluca[2] and Henry F. Diaz[3]

Journal of Geophysical Research – Atmospheres, 2014

[1] Department of Atmospheric and Environmental Sciences, University at Albany, ES 316A, 1400 Washington Avenue, Albany, NY 12222 (oelisontimm@albany.edu)

[2] Department of Geography, University of Hawai‘i at Mānoa, 2424 Maile Way, Honolulu, HI, 96822, USA

[3] NOAA/ESRL Cooperative Institute for Research in Environmental Sciences, University of Colorado, Boulder, Colorado, USA.

## 1. Introduction

In this supplementary section we provide additional information on the climatological mean rainfall pattern in Hawai‘i. Further, we illustrate our discussion of the stationarity assumption that underlies our statistical downscaling method with two supplementary figures. First, a geometric interpretation of how future changes in the teleconnection pattern could affect the downscaled precipitation results. Second, we try to obtain insight into the stationarity assumption from CMIP5 model data itself. For this purpose we assumed that the CMIP5 model rainfall over grid boxes in the Hawaiian Island region are reasonable proxies for studying the stationarity of teleconnection pattern. We did not test how similar the derived composite pattern are with respect to the rainfall station's composite pattern, but instead looked at the relative changes in the composite pattern between the historical 20$^{th}$ century simulations and the future mid and late 21$^{st}$ century simulations in the two scenarios RCP4.5 and RCP8.5. We worked with a smaller subset of the 32 CMIP5 models listed in Table 2 in the main text. This does not affect the results presented here.

## 2. Precipitation climatology

The statistical downscaling of seasonal mean rainfall changes works exclusively with rainfall percentages. The seasonal mean rainfall climatology that we used here as a reference value refers to the average rainfall amounts of the years 1978–2007. The wet season rainfall (November-April) and dry season (May-October) climatologies were derived from monthly gap-filled monthly mean station data of the Rainfall Atlas of Hawai´i [Giambelluca et al., 20013] (http://rainfall.geography.hawaii.edu/). A geospatial interpolation method (Kriging) was used to derive the interpolated map surfaces from irregularly spaced station data points. We provide in

Figure 1 the maps with the climatological seasonal mean rainfall. We note that these seasonal climatologies are not part of the official Rainfall Atlas of Hawai‘i. The gridded data sets are available from the corresponding author upon request.

## 3. Geometric considerations associated with the stationarity assumption

We derived empirical relationships between local rainfall and large-scale circulation using information from the covariance structure among rainfall stations and large-scale climate. The composite method adopted in this study is a means to cluster the large-scale circulation conditionally dependent on the local rainfall. The resulting pattern from the high-precipitation and low-precipitation subsamples and their differences form a set of teleconnection patterns, in which a change in one random variable at one location is associated with changes in a geospatial field represented by a random vector variable.

A key step in our statistical downscaling method is the projection of future changes in the geospatial field onto these teleconnection patterns, which are assumed to be stationary in time.

This way we measure the correlation and the amplitude of the climate change pattern relative to the teleconnection pattern:

$$p_0 = \frac{\langle \vec{y}, \overrightarrow{x_0} \rangle}{|\overrightarrow{x_0}|} = \langle \vec{y}, \overrightarrow{e_0} \rangle$$

Here $\overrightarrow{x_0}$ and $\overrightarrow{y}$ are n-dimensional vectors representing the teleconnection pattern at present day and a future climate change pattern, respectively. The dimension of the vector space is given by the spatial grid (25x21) in our case. Note that the vector projection uses unit-length vectors $\overrightarrow{e_0}$ for the projection direction (by dividing the vector-product by the length of the teleconnection vector $|\overrightarrow{x_0}|$ (see Figure 2)). Note that a climate change vector orthogonal to a teleconnection pattern

would lead to a projection index equal to zero and thus would not induce any change in the estimated rainfall anomalies.

If the teleconnection pattern changed in future, differences between high and low precipitation anomalies would be associated with a future projection direction that is given by $\overrightarrow{e_f}$. In the illustrated example (Figure 2) a large change in the spatial teleconnection pattern is implied. Together with the particular direction of the climate change vector, this example shows a case, where indeed the bias from using stationarity assumption would be severe. The true projection index is given by

$$p_f = \frac{\langle \vec{y}, \overrightarrow{x_f} \rangle}{|\overrightarrow{x_f}|} = \langle \vec{y}, \overrightarrow{e_f} \rangle$$

Since the climate change signal and the original teleconnection vector form a wide angle (low spatial correlation) and since the change in the teleconnection pattern is large and pointing away from the climate change vector, the net result is a much smaller signal amplitude and even a change in the sign. The bias induced by the stationarity assumption is

$$\Delta p = p_0 - p_f = \langle \vec{y}, \overrightarrow{e_0} \rangle - \langle \vec{y}, \overrightarrow{e_f} \rangle = \langle \vec{y}, (\overrightarrow{e_0} - \overrightarrow{e_f}) \rangle = \langle \vec{y}, \vec{d} \rangle$$

Note that difference vector $\vec{d}$ between the present-day and future projection direction vectors consists of a vector component parallel and orthogonal to the present-day projection direction vector. Thus $\vec{d}$ can be expressed as a linear combination of $\overrightarrow{e_0}$ and an orthogonal direction vector $\overrightarrow{e_{0\perp}}$. Therefore the bias or error induced by the stationarity assumption of a single projection pattern (single direction vector) is:

$$\Delta p = s\langle \vec{y}, \overrightarrow{e_0} \rangle + r\langle \vec{y}, \overrightarrow{e_{0\perp}} \rangle .$$

The first term on the right hand side is a scaling error, which by itself suggests (s<1) that we would overestimate the precipitation anomaly. However, this can be easily compensated for by the second term. It is clear that the change in the circulation ($\vec{y}$) and in the teleconnection pattern determine the final bias of the results. In our illustrated example, the difference vector lines up more closely with the climate change direction vector, leading to a positive bias in the projection index and even a reversed sign compared with the true projection index $p_f$.

Finally, we point out that we used a multivariate set of teleconnection patterns, which could have a cancelling effect or reinforcing effect on the individual errors. Further investigations will be needed to develop more robust statistical downscaling methods for coping with non-stationary teleconnection patterns. Furthermore, a change in the teleconnection pattern in future climate would only affect the projection index through change in the direction of vector $\vec{x}$ not by changes in the amplitude of the teleconnection itself. However, the projection index is the basis of the predictor information that is translated into rainfall anomalies through a PCA-based multiple linear regression model. These MLR regression coefficients are scaling factors that translate the projection indices into precipitation anomalies. The regression coefficients are again assumed stationary in time, and thus a scaling error would be the implicit consequence of this second stationarity assumption.

## 3. Taylor-diagram for descriptive analysis of the stationarity in teleconnection pattern.

Taylor-diagrams depict the spatial correlation between two vectors and the standard deviation ratio of the two vectors. Here, we used the Taylor-diagram as a descriptive tool to compare the modeled teleconnection pattern. The historical runs from 24 CMIP5 models were used to define

104 a ‘present-day’ teleconnection pattern. To this end, the six grid boxes encompassing the region of
105 the main Hawaiian Islands were averaged into a wet season precipitation index. This index was
106 used to form high and low precipitation composites with the large-scale circulation fields (here
107 we show only the 500 hPa geopotential height results). Likewise, we analyzed the future
108 teleconnection pattern using the RCP4.5 and RCP8.5 scenario years 2040–2070 and 2070–2099.
109 This way we obtain a first qualitative view on the stationarity of the teleconnection pattern.

110 The results show that the teleconnection patterns already have a large range of variability in the
111 historical runs, when the sampling window is slightly shifted. This indicates that the
112 teleconnection pattern is rather weak, or that the chosen geographic domain is too large and
113 includes a number of grid points that are physically independent in the Hawaiian region. It is also
114 a measure of the sampling variability (resulting from 30-year samples), since we cannot expect a
115 fully deterministic relationship between rainfall anomalies and 500 hPa geopotential height
116 fields. We tested additional combinations with moisture transports and also specific humidity as
117 index and field variable. Similar ranges of spread were observed. With the knowledge of this
118 large range of uncertainty in the last 50 years of the historical runs, the future scenarios show
119 some decrease in the overall spatial correlation and some increase in the overall spread. Thus, the
120 average distance from the ‘optimal point’ in the Taylor-diagram is growing in the future
121 warming experiments. This suggests that the teleconnection pattern might change systematically
122 in future.

123

## References

Giambelluca, T.W., Q. Chen, A.G. Frazier, J.P. Price, Y.-L. Chen, P.-S. Chu, J.K. Eischeid, and D.M. Delparte, 2013: Online Rainfall Atlas of Hawai‘i. *Bull. Amer. Meteor. Soc.* 94, 313-316, doi: 10.1175/BAMS-D-11-00228.1.

## Figures

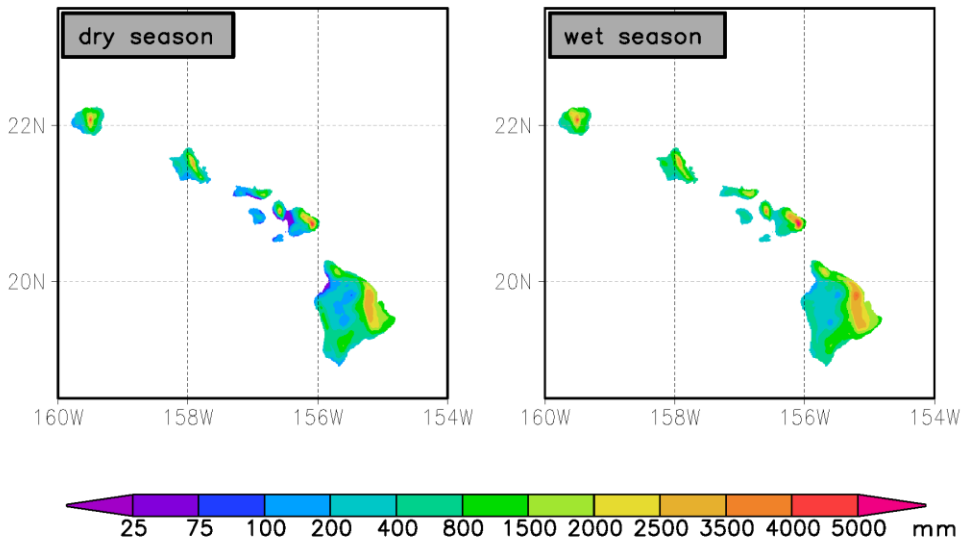

Figure 1: Seasonal mean rainfall climatologies for the dry and wet season (derived from seasonal-mean station data averaged over years 1978-2007).Wet and dry season rainfall is the amount of rain falling in the months November-April and May-October, respectively.

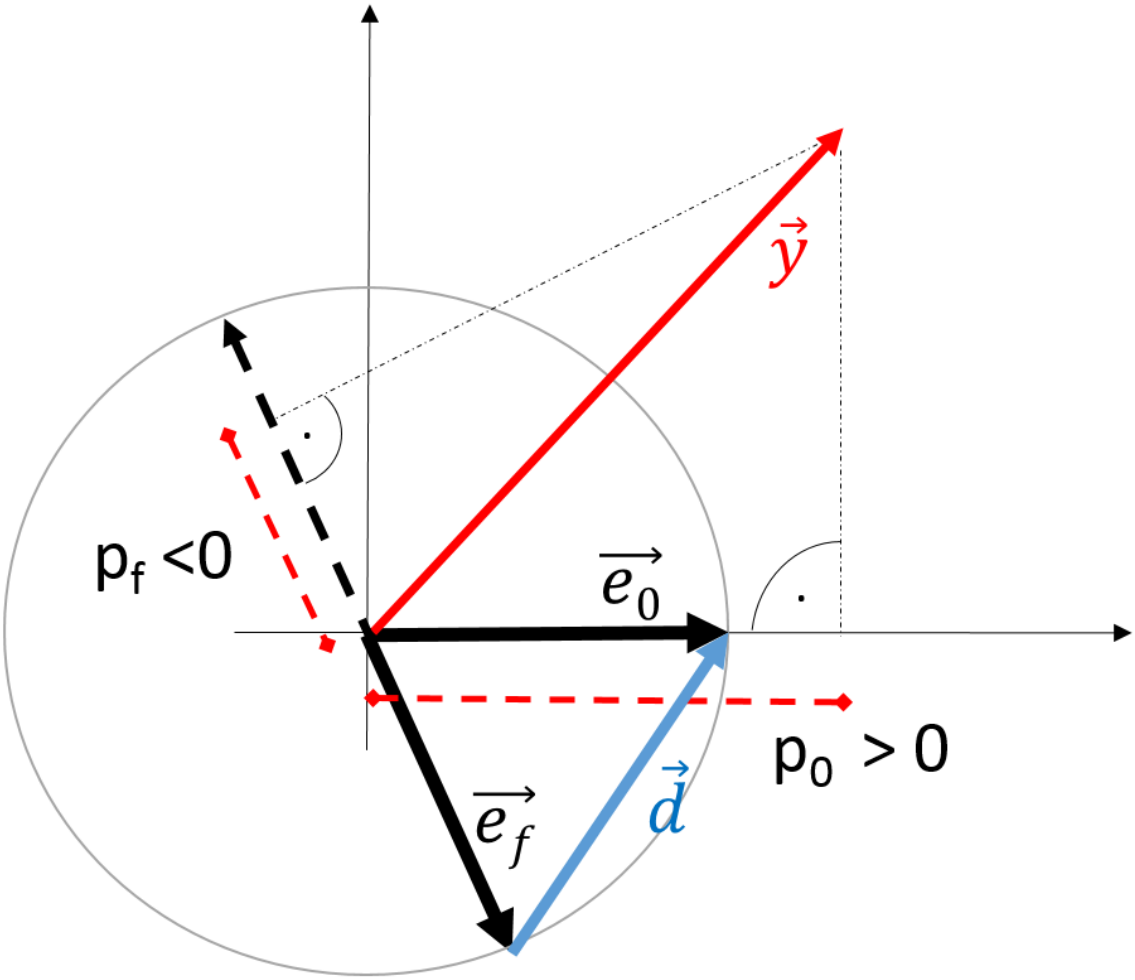


Figure 2: Geometric illustration of the effects of changes in the teleconnection pattern on the projection index used for precipitation downscaling. See text for details.

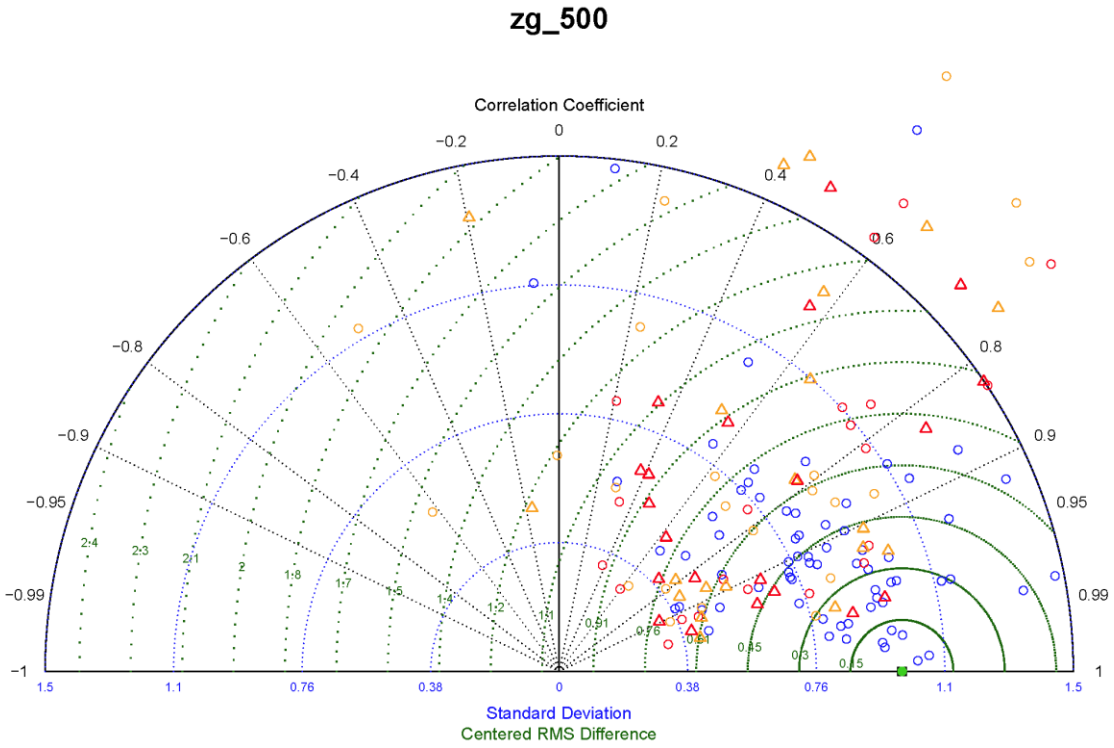


Figure 3: Taylor diagram for testing the stationarity assumption in the CMIP5 simulated teleconnection pattern between wet season rainfall in the geographic area over Hawai‘i and 500 hPa geopotential fields. Blue symbols show the comparison of 1955-1985, 1965-1995, and 1985-2005 teleconnection pattern and the ‘present-day’ 1975-2005 reference teleconnection patttern. Orange and red symbols depict the comparison of the modeled future teleconnection pattern (years 2040-2070 and 2070-2099, respectively). Open circles represent the RCP4.5 scenario, traingles are the results from the RCP8.5 scenario. Note 24 of the models in Table 2 were used in this analysis.